1094

THESE

présentée à
LA FACULTE DES SCIENCES
UNIVERSITE DE NEUCHATEL

pour l'obtention du grade de
DOCTEUR ES SCIENCES

par

E.A.H. ZUUR
Ingénieur-mathématicien diplômé
de la Technische Hogeschool Delft

MODELING OF GENERAL CIRCULATION PROCESSES IN LAKE AND MARINE SYSTEMS AND THEORETICAL SUSPENDED PARTICLE DISTRIBUTIONS IN THE OPEN OCEAN

Soutenue le 11 Octobre 1990, devant la Commision d'Examen:

MM. F.NYFFELER ..... Président
O.BESSON .....
B.KUEBLER ..... } Examinateurs
E.MITTELSTAEDT .....
G.L.WEATHERLY .....

- 1990 -

IMPRIMATUR POUR LA THÈSE

Modélisation des processus de circulation générale dans des systèmes lacustres ou marins et distributions théoriques des particules en suspension en océan ouvert

de Monsieur Eduard A.H. Zuur

UNIVERSITÉ DE NEUCHÂTEL

FACULTÉ DES SCIENCES

La Faculté des sciences de l'Université de Neuchâtel sur le rapport des membres du jury,

Messieurs F. Nyffeler, B. Kubler, O. Besson, G. Weatherly (Tallahassee, Floride) et E. Mittelstädt (Hambourg)

autorise l'impression de la présente thèse.

Neuchâtel, le 26 novembre 1990

Le doyen:

Cl. Mermod

Voor mijn ouders

"'Then,' said Glorfindel, 'let us cast it into the deeps (...): In the sea it would be safe.'

'Not save for ever,' said Gandalf. 'There are many things in the deep waters; and seas and lands may change. And it is not our part here to take thought only for a season, or for a few lives of Men, or for a passing age of the world. We should seek a final end of this menace, even if we do not hope to make one.'"

J.R.R. Tolkien, The Lord of the Rings

TABLE OF CONTENTS

PREFACE 1

INTRODUCTION 3

1. Objectives 3

2. Modeling of mesoscale circulation processes 5

2.1. The Sandia Ocean Modeling System 5

2.2. The PROSPER General Circulation Model 6

2.3. A numerical simulation of meso-scale dispersion 6

3. Theoretical suspended particle distributions in open ocean systems 7

GENERAL CONCLUSION 8

REFERENCES 10

PAPERS:

Zuur, E.A.H., and D.E.Dietrich, 1990. The SOMS model and its application to Lake Neuchâtel. Aquatic Sciences 52/2.

Zuur, E.A.H., 1990. The Prosper General Circulation Model, a Numerical Description. Int. J. Num. Meth. Fluids (in press).

Zuur, E.A.H., G.L. Weatherly and F. Nyffeler, 1990. A numerical simulation of mesoscale dispersion in the deep ocean. Manuscript.

Zuur, E.A.H., and F. Nyffeler, 1990. Theoretical suspended particle distributions in open ocean systems; a comparison with observations. Submitted to Deep-Sea Research.

PREFACE

The present work consists of four papers. The first three are concerned with the development and appliclation of a general meso-scale circulation model. In the fourth paper theoretical suspended particle distributions in open ocean systems are derived and compared with observations. The research was performed within the framework of the PROSPER program at the University of Neuchâtel with the support of the Swiss Environmental Protection Office and the Swiss National Science Foundation.

I'am grateful to Dr. François Nyffeler, director of the PROSPER research group and of this thesis, for his guidance of the work. Had he not realized the importance of and argued for a mathematical modeling approach in order to gain understanding of transport processes occuring in the deep-sea, this project would never have been started. He is co-author of two of the presented papers, and his remarks helped improving the other two manuscripts.

Prof. Bernard Kübler was a great support. By having my office next to his, I was able to benifit a lot from his scientific experience. Dr. David Dietrich of Sandia National Laboratories introduced me to the concepts used in geo-physical modeling. His ocean-scale circulation model formed the starting point for the meso-scale model that has been developed in Neuchâtel. Prof. George Weatherly made me aware of the complexity and multitude of subjects in physical oceanography during the period of time I was at Florida State University. Prof. Olivier Besson has put me back on the right track, when I was trapped by the difficulties I encountered in developing the PGCM model. Dr. Ekki Mittelstaedt made several critical remarks on the proofs of the manuscript that helped improving the final version. I would like to express my gratitude to each of them.

Colleagues at the institute whose help on different occasions was indispensable, are Thierry Adatte, Carlos Beck, Xavier Durrieu de Madron, Charles-Henry Godet, Rüdiger Jantschik, Rachid Laydi, Patrick Ruch and George Rumley.

This work would not have been possible without modern computer facilities. The VAX system at the University of Neuchâtel and the supercomputer CRAY-II at the Ecole Polytechnique Fédéral in Lausanne were indispensable tools in order to perform the necessary calculations. I thank the calculation centre of the University of Neuchâtel for their effectiveness in making these tools accessible.

Finally, my parents, my sisters, Susanne and Arno were a great help in many ways and their influence is reflected in this manuscript in one way or another.

INTRODUCTION

The present work has been carried out in the framework of the "Programme de Recherches Océanographiques Suisse Pour l'Elimination des Radionucléides" (PROSPER) at the university of Neuchâtel. PROSPER was established in 1981, in order to fulfil the demand of the Swiss government to survey the Dumpsite for low-level radioactive waste in the North-east Atlantic Ocean and to study related physical processes. PROSPER represents Switzerland as a member of the Coordinated Research and Environmental Surveillance Programme (CRESP). To collect relevant data, PROSPER participated in a number of field programs, such as the Nordost Atlantisches Monitoring Programm (NOAMP).

1. Objectives

In studying the dispersion of dissolved or particulate material from a source at the ocean-floor a number of stages can be identified (Robinson, 1985). The first stage takes place in the benthic boundary layer (BBL). The BBL is the layer of water adjacent to the ocean bottom in which the vertical gradient of potential temperature is significantly smaller than in the deep-ocean interior. Its thickness varies between 30 and 100 m. Boundary-generated small-scale turbulence gives rise to intensive vertical and horizontal mixing of the fluid inside the BBL on time-scales small compared to those in the interior of the ocean (D'Asaro, 1982). In the second stage dispersive processes by mesoscale processes begins, and material is sucked out of the BBL and transported into the ocean interior. In the third stage dispersion to basin and larger scales takes place by eddy diffusivity into isopycnal surfaces that outcrop at the sea surface at higher latitudes.

In the last decades more measurements and knowledge have

become availabe concerning mesoscale processes in the ocean (Robinson, 1983). In particular, it was observed that meso-scale processes may be very energetic near the bottom of the ocean (Mittelstaedt 1986, Klein 1987). The interaction of strong near bottom currents with topography induces meso-scale whirl-like circulation structures (eddies), by which vertical transport is provoked. Eddies may thus establish a short circuit for material at the bottom to rise to a much higher level in a relatively short time.

Since most studies of the CRESP members were mainly concerned with the dispersion of contaminated material on a ocean-wide scale, it was decided that in Neuchâtel local near-site dispersion processes would be the object of study. In particular vertical transport of dissolved and particulate material from the turbulent bottom boundary layer into the interior of the deep ocean by advection and diffusion is regarded as a main subject of interest.

Interpretation of the hydrographic data, obtained during the NOAMP campaigns near the Dumpsite area in the Northeast Atlantic, demanded for a mathematical modeling approach of regional meso-scale processes in the deep ocean. The model to be applied should relate the data to the vertical transport of material from the bottom, a transport process which is not accessible to direct observations. Two specific objectives were put forward:

- The development and application of a regional, high-resolution general circulation model in order to simulate meso-scale circulation processes and the resulting dispersion of dissolved or particulate material from the ocean bottom.
- A theoretical support for the observed general trends of suspended particle distributions in open ocean systems, in particular near the Dumpsite region for low level radio-active waste.

The first three of the presented papers are concerned with the first objective. The first paper deals with the mathematical

analysis and a case-study of an existing model that was originally developed to simulate large-scale circulations. By taking this model as a starting point, a meso-scale circulation model has been developed in Neuchâtel. The description and analysis of this model is presented in the second paper. In the third paper the later model is applied to simulate a relevant meso-scale circulatation process and the resulting dispersion of material from a source at bottom. The fourth paper is concerned with the second objective. In this study theoretical suspended particle distributions are derived and compared with observations.

2. Modeling of mesoscale circulation processes

2.1. The Sandia Ocean Modeling System

The Sandia Ocean Modeling System (SOMS) is a three dimensional ocean-circulation model, developed at Sandia National Laboratories in Albuquerque by Dietrich, Marietta and Roache (1987). It is based on the incompressible Navier-Stokes equations, the mass-conservation equation, an equation of state and the heat-equation. The hydrostatic approximation is used. Numerical treatment of the equations is performed with a finite difference method. Specific features of the SOMS model are the use of an equivalent formulation of the incompressible Navier-Stokes equations and the mass-conservation equation, implicit treatment of the Coriolis term in the finite difference scheme, and the predictor-corrector method inside a time-step in order to determine the new velocity components and surface pressure.

In 1988 a cooperative effort between PROSPER and Sandia National Laboratories was started in order to validate the SOMS model in simulating meso-scale circulation processes. The interest at the University of Neuchâtel in the general circulation in Lake Neuchâtel, the lake's pronounced topography and the suitability of its dimension made us apply the model to this lake under barotropic conditions. The SOMS model and its application to Lake

Neuchâtel are described by Zuur and Dietrich (1990).

2.2. The PROSPER General Circulation Model

Implicit treatment of the Coriolis term is useful in case ocean-scale processes are simulated, because it permits a bigger time-step. On smaller scales, however, explicit treatment of this term does not imply additional stability requirements. A drawback of the implicit treatment of the Coriolis term in SOMS is that it introduces numerical diffusion in the integration scheme, which diffusion increases if the time-step decreases. This makes it difficult to simulate circulation processes with thermal stratification, since then the time-step may be limited strongly by internal wave propagation. Therefore, in case of simulating meso-scale circulation processes this term is better treated in an explicit way. The predictor-corrector method in SOMS is valid only in case of Neumann boundary conditions. Although Neumann conditions are often used in geophysical circulations problems, they may result in a 'drift' of the calculated results. To allow for Dirichlet conditions as well, an extended version of the predictor-corrector method was developed in Neuchâtel. The adaptation of the SOMS model leaded to the development of the PROSPER General Circulation Model (Zuur, 1990).

2.3. A numerical simulation of meso-scale dispersion

A benthic storm is loosely defined as a state in which the velocities near the bottom of the deep ocean are greater than 10 cm/s, and that lasts at least 48 hours. By tracing deep sea floats, numerous benthic storms were detected during the NOAMP field campaigns (Klein, 1987). During these missions the PROSPER group collected the hydrographic data. It was observed that most storms had a whirl-like structure and were obviously closely related to deep-reaching eddies. The average diameter of these eddies was found to be of the order of the local baroclinic Rossby

deformation radius, being about 70 km. Besides the fact that benthic storms are energetic flows by definition, time series of current measurements indicate that they are by no means exceptional, but exist a great deal of time.

The PGCM was used to simulate such a benthic storm. The topography of the Dumpsite area and thermal stratification were included in the model. The aim of this study was to investigate the combined effect of benthic storms and topography on the vertical dispersion of a dissolved tracer from a source at the bottom of the ocean. It is shown that significant vertical mixing of material over a height of several hundreds of meters takes place on a time-scale of days. This study is presented in Zuur, Weatherly and Nyffeler (1990).

3. Theoretical suspended particle distributions in open ocean systems

Over three-hundred nephelometric profiles have been obtained at and around the Dumpsite area during the NOAMP experiment between 1982 and 1985. They have been described by Nyffeler and Godet (1986). These profiles measured by continous optical profiling exhibit a similar trend as those observed in large areas of the open ocean. This trend may be described as a strong decrease with depth directly below the biologically active surface layer, a further decrease with an almost constant gradient down to the clear water minimum level, and then an increase of the turbidity towards the bottom.

In the last paper of this report (Zuur and Nyffeler, 1990) a theoretical support is given for the observed trend of the nephelometric profiles. A mathematical model is presented to determine the number of particles per unit volume and the particle size-distributiuon as functions of depth, when this number and this distribution are prescribed at the surface and/or at the bottom. The influence of dissolution, absorption, splitting and

aggregation of particles is assessed, and theoretical nephelometric profiles are derived. Comparison with data demonstrates that the effect of dissolution alone, in connection with the dynamical behaviour of the particles, is sufficient to restore the general trend of the experimental profiles. In particular, remobilisation of small particles from the benthic boundary layer and their subsequent dissolution would be sufficient to explain the thickness of the nepheloid layer below the clear water minimum level.

GENERAL CONCLUSION

The heart of the problem with which the PROSPER group is concerned, is an analysis of the possible consequences for our environment of the dumping of low-level radioactive waste in the Northeast Atlantic. This analysis must be performed on a interdisciplinary basis, since the many aspects that are involved, relate to different fields of study, among which biology, chemistry, physics and oceanography. In this thesis specific oceanographical aspects have been considered.

Two major parts of the presented work are the development of a meso-scale general circulation model and a mathematical formulation of the dynamical behaviour of particulate matter in the ocean. These parts may be of interest to a broader field of study in marine science than the one only concerned with the problematic of the dumping of low-level radioactive waste. Therefore, these parts were presented and discussed in the papers on their own, independent of this specific problematic.

By developing the models we aimed to realistically simulate important transport processes in the ocean. In particular vertical dispersion of material formed a subject of interest. It is clear, that understanding and quantification of such processes are indispensable in assessing ecological impacts resulting from deep-sea disposal of any kind of potentially harmful material. By

applying the circulation model we were able to quantify the meso-scale dispersion of dissolved material from the benthic boundary layer that is provoked by a frequently occuring transport mechanism in the ocean. By studying the dynamical behaviour of particulate matter a better understanding of observed particle distributions in the ocean could be obtained, and by comparing theoretical results with observations information about regional, long-term, mean upward vertical transport of particulate matter could be derived.

Because of the limited memory-capacity and computation-speed of existing computers, the models used to date to perform ocean-scale impact assessments are not able to resolve meso-scale processes explicitly, but instead use a turbulent closure scheme by which the influence of these processes on the large scale circulation is parametrized. By its outcomes, the present work shows that dispersion on a meso-scale may be considerable. This implies the importance to embedding meso-scale effects as good as possible into large-scale circulation models, in order to simulate ocean-wide dispersion of material in the most realistic way. A question that should be answered in the near future, is whether and how the incorporation of these effects may be improved.

REFERENCES

Abdallah, S., and J.Dreyer, 1988. Dirichlet boundary conditions for the pressure poisson equation of incompressible flow. Int. J. Num. Meth. in Fluids, Vol.8, 1029-1036.036.

Arakawa, A. and V.R.Lamb, 1977. 'Computational design of the basic dynamical processes of the UCLA general circulation model', Methods in Computational Physics, Vol.17, Academic Press, pp. 174-265

Bader H. (1970). The hyperbolic distribution of particle sizes. Journal of Geophysical Research, 75, 2822-2830

Bapst, A., 1987. Le Lac de Neucâtel: thése présentée a la Faculté des Sciences (université de Neuchâtel).

Batchelor G.K. (1967). An Introduction to Fluid Dynamics, Cambridge University Press.

Besson, O., and R.Laydi. Some estimates for the hydrostatic approximation, and for the anisotropic Navier-Stokes equations. In preparation.

Biscaye P.E. and S.L. Ettreim (1977). Suspended particulate loads and transports in the nepheloid layer of the abyssal Atlantic. Marine Geology, 23, 155-172.

Brewer P.G., D.W.Spencer, P.E.Biscaye, A.Hanley, P.L.Sachs, C.L.Smith, S.Kadar and J.Fredericks (1976). The Distribution of Particulate Matter in the Atlantic Ocean. Earth and Planetary Science Letters, 32, 393-402.

Brun-Cottan J.C. (1971). Etude de la granulométrie des particule marines, mesures effectuées avec un compteur Coulter. Cahier Océanographiques, 23, 193-205

Brun-Cottan J.C. (1976). Stokes settling and dissolution rate model for marine particles as a function of size distribution. Journal of Geophysical Research, 81, N°9, 1601-1606.

Bryan, K., 1969. A numerical method for the study of the circulation of the world ocean. J.Comp.Phys.,4,347-376.

D'Asaro, E., 1982. Velocity structure of the Benthic Ocean. J.

Phys. Oceanog, 12, 323-336.

Dietrich, D.E., B.E.McDonald and A.warn-Varnas (1975). Optimized Block-Implicit Relaxation. J. Comp. Phys.,18,421-439.

Dietrich, D.E., M.G.Marietta and P.J.Roache, 1987. 'An Ocean Modeling System with Turbulent Boundary Layers and Topography', International Journal for Numerical Methods in Fluids, vol.7, 833-855.

Ettreim S.L, E.M.Thorndike and L.Sullivan (1976). Turbidity in the Atlantic Ocean. Deep-Sea Research, 23, 1015-1027.

Gresho, P.M., and R.L.Sani, 1987. On pressure boundary conditions for the incompressible Navier-Stokes equations. Int. J. Num. Meth. in Fluids, Vol.7, 1111-1145.

Hutter, K., 1984. Mathematische Vorhersage von barotropen und baroklinen Prozessen im Zürich- und Luganersee. Vierteljahresschrift der Naturforschenden Gesellschaft in Zürich. 129:51-92.

Klein H. (1987). Bentic Storms, and Particle Dispersion in the Deep West European Basin. Dt.hydrogr.Z.40.

Lal D. (1977). The Oceanic Microcosm of Particles. Science, Vol.198, Nr.4321, 997-1009.

Lambert C.E., C.Jehanno, N.Silverberg, J.C.Brun-Cottan and R.Chesselet (1981). Log-normal distribution of suspended particles in the open ocean. Journal of Marine Research, 39, 77-98.

Lerman A., D.Lal and M.F.Dacay (1974). Stokes' settling and chemical reactivity of suspended particles in natural waters. in: Suspended Solids in Water, edited by R.J.Gibbs, pp. 17-47, Plenum, New York.

Lerman A., K.L.Cardner and P.R.Betzer (1977). Elimination of fine suspensoids in the oceanic water column. Earth and Planetery Science Letters, 37, 61-70.

McCave I.N. (1975). Vertical flux of particles in the ocean. Deep-sea Research, 22, 491-502.

McCave I.N. (1983). Particulate size spectra, behaviour and origin of nepheloid layers over the Nova Scotian Continental Rise. Journal of Geophysical Research, 88, 7647-7666.

McCave I.N. (1984). Size spectra and aggregation of suspended

particles in the ocean. Deep-Sea Research, Vol 31, N°4, 329-352.

Mellor, G.L., and T.Yamada, 1982. Development of a Turbulence Closure Model for Geophysical Fluid Problems. Reviews of geophysics and space physics. 20,851-875.

Mittelstaedt, E., M.Bock, I.Bork, H.Klein, H.Nies, U.Schauer,1986. 'Ausbreitungsbedingungen für Stoffe in grossen Tiefen (NOAMP-Nordostatlantisches Monitoring-Programm)', Hamburg: Deutsches Hydrogr. Institut. 202 S.m.Abb.u. Tab.

Morel A. (1973). Diffusion de la lumière par les eaux de mer. Résultat expérimentaux et approche théorique. in: Optics of the Sea/ Lectures serie 61/ 3.1.1-3.1.76, AGARD-NATO Brussels.

Nyffeler F. and C.H.Godet (1986). The structural parameters of the benthic nepheloid layer in the Northeast Atlantic. Deep-Sea Research, 33, 2, 195-207.

Nyffeler F. and P.Ruch (1989). Size distribution of the suspended particles in the water masses of the Northeast Atlantic. in: Interim oceanographic description of the North-East Atlantic dumpsite for radioactive waste / OCDE Paris, 1989.

Pak H., J.R.V.Zaneveld and J.Kitchen (1980). Intermediate nepheloid layers observed off Oregon and Washington. Journal of Geophysical Research, 85, 6697-6708.

Pedlosky, J.,1987. 'Geophysical Fluid Dynamics', Springer Verlag New York.

Orlanski, I., 1976. 'A simple boundary condition for unbounded hyperbolic flows', J. Comp. Physics, 21, 251-269.

Richards, K.J., 1986. 'Dispersion of tracers by the oceanic eddy field'. Inst. of Ocean. Sciences, Wormley, I.O.S. report No. 229

Roache, P.J., 1978. Marching methods for elliptic problems. Num. Heat. Transfer, Vol.1, 1-25(Part 1), 163-181(Part 2) and 183-201 (Part 3).

Roache, P.J., 1982. Computational fluid dynamics. Hermosa.

Roache, P.J., and D.E. Dietrich, 1988. Evaluation of the filtered leapfrog-trapezoidal time integration method. Numerical Heat Transfer.

Robinson, A.R., 1983. Eddies in Marine Science. Springer-Verlag, Berlin, Heidelberg, New York, Tokyo.

Robinson, A.R. and S.L. Kupferman, 1985. 'Dispersal from deep ocean sources: Physical related processes', Sandia-report, SAND82-1986.

Semtner, A.J. An oceanic general circulation model with bottom topography',NTIS PB 276 840.

Sheldon R.W., A.Prakash and W.H.Sutcliffe (1972). The size distribution of particles in the ocean. Limnology and oceanography, 17, 327-340.

Sollberger, H., 1974. Le Lac de Neuchâtel: thèse présentée a la Faculté des Sciences (Université de Neuchâtel).

Welsch, J.E., F.H. Harlow, J.P. Shannon and B.P. Daly, 1966. The MAC Method, LA-3425. Los Alamos, New Mexico.

Zuur, E.A.H., and D.E.Dietrich, 1990. The SOMS model and its application to Lake Neuchâtel. Aquatic Sciences 52/2.

Zuur, E.A.H., 1990. The Prosper General Circulation Model, a Numerical Description. Int. J. Num. Meth. Fluids (in press).

Zuur, E.A.H., G.L. Weatherly and F. Nyffeler, 1990. A numerical simulation of mesoscale dispersion in the deep ocean. Manuscript.

Zuur, E.A.H., and F. Nyffeler, 1990. Theoretical suspended particle distributions in open ocean systems; a comparison with observations. Submitted to Deep-Sea Research.

Aquatic Sciences 52/2, 1990

1015-1621/90/020115-15 $ 1.50 + 0.20/0

The SOMS model and its application to Lake Neuchâtel

E. A. H. Zuur [1] and D. E. Dietrich [2]

[1] PROSPER, University of Neuchâtel, Switzerland
[2] Sandia National Laboratories, Albuquerque, New Mexico

Key words: Conservative primitive equations; general circulation model.

ABSTRACT

A three-dimensional numerical circulation model (SOMS) based on primitive equations is described. The algorithm, by which Coriolis and vertical diffusion terms are treated implicitly while mass is still conserved exactly (algebraically), is discussed in detail. The model is applied to Lake Neuchâtel (Switzerland), to determine the general circulation under influence of the most prevailing wind.

1. Introduction

Mathematical computer models are currently being used with relevant observations to assess transport and dispersion of soluble and suspendable materials in lakes and oceans, originating from various sources. The model that is described in this paper is a three dimensional numerical circulation model based on primitive equations. Originally it was developed for ocean studies at Sandia National Laboratories in Albuquerque, and is referred to as the SOMS model (Sandia Ocean Modelling System). The model has advantageous stability characteristics and the operation-count per time step is relatively small compared with other 3D methods (see Dietrich, 1987). Therefore, a high resolution of the computational grid is possible. The model is applied to Lake Neuchâtel (Switzerland), to provide a first overview of the general circulation induced by the most prevailing wind.

This paper includes a description of the SOMS model and illuminates in particular the specific predictor-corrector scheme by which the surface pressure is determined and the part of the algorithm that treats Coriolis and vertical diffusion implicitly, while mass is still exactly conserved in the algebraic sense. Further, results of applying the model to Lake Neuchâtel under barotropic conditions are presented.

2. The continuum equations

2.1 Hypotheses and approximations

The Navier-Stokes (N-S) equations, a set of non-linear partial differential equations, together with an equation of state, an energy equation, and appropriate boundary and initial conditions govern Newtonian fluids (see Batchelor, 1967). The special nature of the Lake problem allows certain approximations that are used to simplify the governing equations. The resulting system is integrated using a fast computer such as a CRAY-2. Scaling estimates of the terms that appear in the N-S equations justify the following approximations (Pedlosky, 1987):

- The Boussinesq approximation: density variations are neglected in the horizontal momentum and mass conservation equations, but are taken into account when they are associated with buoyancy forces (in the vertical momentum equation). Density is assumed independent of pressure and varies only with temperature.
- The hydrostatic approximation: all terms in the vertical momentum equation are neglected except the buoyancy and pressure gradient terms.
- The f-plane approximation: a Cartesian coordinate system attached to the earth with constant Coriolis parameter.
- The rigid lid approximation (see below).
- A relatively simple turbulence closure scheme (see below).

Two categories of water motion can be distinguished, namely the gravitational response and the non-divergent response. The gravitational response is characterized by divergent motion, with a significant ratio of potential to kinetic energy. The time-scale of this response is proportional to the length of the lake divided by the speed of the long gravity waves (the seiche period). It is in the order of minutes for Lake Neuchâtel. For the non-divergent response, however, most of the energy is kinetic and the time-scale is larger than the seiche period. The rigid lid (non-divergent) model which is applied here therefore simulates the transient, large scale circulation in the Lake.

When the equations are solved on a finite space-time domain, the molecular diffusion becomes negligible compared to turbulence effects at a scale smaller than the grid-size of this domain. Although variations at this scale are not resolved by the model, their effect on the resolved motion is important through non-linear interactions. The usual way to account for this effect is to decompose all variables into a mean value and a fluctuating value. Then, the resulting set of equations for the mean values, with the effect of the fluctuating part on the mean flow defined by additional model assumptions, has to be solved. Many levels of sophistication can be used to account for this turbulence part (Mellor and Yamada, 1982). Here, we use a rather popular and relatively simple method: the turbulence is represented in the mean flow equations by means of so-called turbulence viscosity coefficients, which are determined by a simple theoretical model (Pedlosky, 1987).

2.2 *The model equations*

The continuum equations used in SOMS are derived from the previous hypotheses and approximations. They are stated below.

The momentum equations:

$$\frac{\partial u}{\partial t} = -\frac{1}{\varrho_0}\frac{\partial p}{\partial x} + fv - \nabla \cdot (u\,\mathbf{v}) + \frac{\partial}{\partial x}\left(A_h \frac{\partial u}{\partial x}\right) + \frac{\partial}{\partial y}\left(A_h \frac{\partial u}{\partial y}\right) + \frac{\partial}{\partial z}\left(A_v \frac{\partial u}{\partial z}\right), \quad (1)$$

$$\frac{\partial v}{\partial t} = -\frac{1}{\varrho_0}\frac{\partial p}{\partial y} - fu - \nabla \cdot (v\,\mathbf{v}) + \frac{\partial}{\partial x}\left(A_h \frac{\partial v}{\partial y}\right) + \frac{\partial}{\partial y}\left(A_h \frac{\partial v}{\partial y}\right) + \frac{\partial}{\partial z}\left(A_v \frac{\partial v}{\partial z}\right). \quad (2)$$

The hydrostatic equation:

$$\frac{\partial p}{\partial z} = \varrho g. \quad (3)$$

The mass conservation equation:

$$\frac{\partial u}{\partial x} + \frac{\partial v}{\partial y} + \frac{\partial w}{\partial z} = 0. \quad (4)$$

The equation of state:

$$\varrho = \varrho_0 (1 - \alpha T). \quad (5)$$

The heat equation:

$$\frac{\partial T}{\partial t} = -\nabla \cdot (T\,\mathbf{v}) + Q(T), \quad (6)$$

in which $Q(T)$ represents sources, sinks, and the diffusive redistribution of T.

The following symbols are used:

x, y, z	spatial coordinates in a left-handed Cartesian system (z-axis points downwards) $[L]$;
t	time $[T]$;
T	(in situ) temperature $[\Theta]$;
u, v, w	velocity components ($\mathbf{v} = (u, v, w)$) $[L\,T^{-1}]$;
p	pressure $[M\,L^{-1}\,T^{-2}]$;
ϱ	density (ϱ_0 is reference density) $[M\,L^{-3}]$;
g	effective gravitational acceleration $[L\,T^{-2}]$;
A_h	horizontal eddy diffusion $[L^2\,T^{-1}]$;
A_v	vertical eddy diffusion $[L^2\,T^{-1}]$;
f	Coriolis parameter $[T^{-1}]$;
α	coefficient of thermal expansion $[\Theta^{-1}]$;
∇	$= (\partial/\partial x, \partial/y, \partial/\partial z)$.

3. Numerical algorithm

The set of continuum equations stated in 2.2 applied to the lake cannot be solved analytically, therefore solutions will be sought numerically. Thus, the space-time domain has to be discretized, and the differential equations must be replaced by algebraic equations for the unknown nodal values of the computational grid.

3.1 Space and time integration

Spatial integration is performed with a finite difference method. The space domain is represented by a finite number of computational points in a 3D-Eulerian computational grid. The grid is regular, but stretched in the vertical coordinate, in order to model accurately the surface and/or bottom boundary layer (Dietrich, 1987). The computational points for different quantities, such as pressure and velocity components, are actually staggered in space (see fig. 1), corresponding to the widely used Arakawa-C grid (Arakawa and Lamp, 1977). The grid cells are considered either wholly inside or wholly outside the lake region. In the remainder subscribts and superscribts indicate spatial- and time-discretization respectively.

For all relevant time dependent quantities the leapfrog method is used in combination with the filtered leapfrog-trapezoidal scheme (FLT) to avoid the tendency of the leapfrog method to decouple solutions at alternate time steps.

In the leapfrog method, as well the time- as the space-derivatives are approximated by centered differences. Consider for convenience only the one dimensional advection equation:

$$\frac{\partial q}{\partial t} = -u\frac{\partial q}{\partial x}, \tag{7}$$

where u is the constant advection velocity. The leapfrog method is:

$$q_i^{n+1} = q_i^{n-1} - c\,(q_{i+1}^n - q_{i-1}^n), \tag{8}$$

in which $c = u\,\Delta t/\Delta x$ is the Courant number (Roache, 1976).

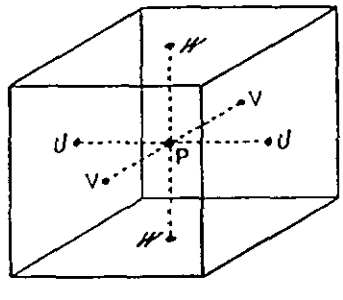

Figure 1. Arakawa-C staggered grid single control volume for pressure. The symbol P denotes the centre of the P-control volume. The symbols U, V and W denote relative positions of control volume centres for horizontal and vertical velocity components

The FLT method consists in substituting q_i^{n-1} in (8) by $(q_i^n + q_i^{n-2})/2$, which actually adds a time filter to the leapfrog method, but does not introduce spatial damping. Let us denote a weighted linear combination of q_i^{n-1} and its filtered value by:

$$\hat{q}^{n-1} = (1-\omega)\, q_i^{n-1} + \omega(q_i^n + q_i^{n-2})/2\,. \tag{9}$$

Combining leapfrog and FLT leads to:

$$q_i^{n+1} = \hat{q}_i^{n-1} - c(q_{i+1}^n - q_{i-1}^n)\,. \tag{10}$$

This integration method is known as the filtered leap-frog-trapezoidal weighted (FLTW) scheme. A description of the properties of the FLTM method is found in Roache and Dietrich (1988).

3.2 Time step procedure

This paragraph describes the overall procedure of one time step. Two specific features of this procedure will be pointed out already: the mass conservation equation is satisfied exactly (algebraically) after every time step; Coriolis and vertical diffusion are treated implicitly for reasons to be discussed in section 3.3.

Before describing the numerical procedure, first some relations are derived from the continuum equations, and some definitions are given. From (3) and (5) it follows that:

$$p = p_s(x, y) + \varrho_0 g z - \varrho_0 g \alpha \int_0^z T(x, y, \zeta)\, d\zeta\,, \tag{11}$$

in which p_s is the surface pressure (p_s is different from the atmospheric pressure due to the rigid lid approximation). Define:

$$L = fv + \frac{\partial}{\partial z}\left(A_v \frac{\partial u}{\partial z}\right), \tag{12}$$

$$M = -fu + \frac{\partial}{\partial z}\left(A_v \frac{\partial v}{\partial z}\right), \tag{13}$$

$$R = g\alpha \int_0^z \frac{\partial T}{\partial x}\, d\zeta - \nabla \cdot (u\, v) + \frac{\partial}{\partial x}\left(A_h \frac{\partial u}{\partial x}\right) + \frac{\partial}{\partial y}\left(A_h \frac{\partial u}{\partial y}\right), \tag{14}$$

$$S = g\alpha \int_0^z \frac{\partial T}{\partial y}\, d\zeta - \nabla \cdot (v\, v) + \frac{\partial}{\partial x}\left(A_h \frac{\partial v}{\partial x}\right) + \frac{\partial}{\partial y}\left(A_h \frac{\partial v}{\partial y}\right). \tag{15}$$

(Note: L and M contain the Coriolis and vertical diffusion terms). Putting (11) to (15) into the momentum equations (1) and (2) yields:

$$\frac{\partial u}{\partial t} = -\frac{1}{\varrho_0}\frac{\partial p_s}{\partial x} + L + R, \tag{16}$$

$$\frac{\partial v}{\partial t} = -\frac{1}{\varrho_0}\frac{\partial p_s}{\partial y} + M + S. \tag{17}$$

Due to the rigid lid approximation, the vertical velocity is zero at the surface. From (4) we obtain:

$$w = \int_0^z \left(\frac{\partial u}{\partial x} + \frac{\partial v}{\partial y}\right) d\zeta. \tag{18}$$

Applying the no-slip condition at the bottom yields:

$$0 = \int_0^h \left(\frac{\partial u}{\partial x} + \frac{\partial v}{\partial y}\right) d\zeta, \tag{19}$$

in which $h = h(x, y)$ is the bottom-depth. By differentiating (16) to x, (17) to y, adding the equations and integrating the result on both sides from surface to bottom (from (19) it follows that the remaining left-hand side is zero), we obtain a 2D Poisson equation for the surface pressure:

$$\frac{\partial^2 p_s}{\partial x^2} + \frac{\partial^2 p_s}{\partial y^2} = \frac{\varrho_0}{h}\int_0^h \left(\frac{\partial L}{\partial x} + \frac{\partial R}{\partial x} + \frac{\partial M}{\partial y} + \frac{\partial S}{\partial y}\right) d\zeta. \tag{20}$$

The numerical procedure can be divided into three parts. The first part makes it possible to treat the L and M terms implicitly when the Poisson equation for the surface pressure is solved. The second part solves this Poisson equation. The third part updates the velocity components and temperature with the resulting surface pressure.

Consider the magnitudes of all time dependent quantities to be known at time $n\Delta t$. The derivation of the magnitudes at time $(n+1)\Delta t$ is described below.

First p_s^{n+1} is approximated by the known p_s^n and the "intermediate" velocity components $\tilde{u}^{n+1}$ and $\tilde{v}^{n+1}$ are calculated from the momentum equations. They serve to evaluate the L and M terms when p_s^{n+1} is calculated from the Poisson equation. They are calculated from the following set of equations:

$$\tilde{u}_{ijk}^{n+1} = \hat{u}_{ijk}^{n-1} + 2\Delta t\left[-\frac{1}{\varrho_0}\frac{\partial p_s^n}{\partial x} + L(\tilde{u}^{n+1}, \tilde{v}^{n+1}) + R^n\right]_{ijk}, \tag{21}$$

$$\tilde{v}_{ijk}^{n+1} = \hat{v}_{ijk}^{n-1} + 2\Delta t\left[-\frac{1}{\varrho_0}\frac{\partial p_s^n}{\partial y} + M(\tilde{u}^{n+1}, \tilde{v}^{n+1}) + S^n\right]_{ijk}, \tag{22}$$

in which:

$$\bar{u}^{n+1} = (\tilde{u}^{n+1} + u^n)/2, \text{ and} \tag{23}$$

$$\bar{v}^{n+1} = (\tilde{v}^{n+1} + v^n)/2\,. \tag{24}$$

The L and M terms are treated implicitly, which means that these terms are also a function of the unknown velocity field components at time $(n+1)\,\Delta t$. The system is solved with appropriate boundary conditions (see section 4), either directly or with a relaxation method.

The second part of the time step procedure solves the Poisson equation using $\bar{u}^{n+1}$ and $\bar{v}^{n+1}$ to determine the L and M terms. With (20) we get:

$$\left[\frac{\partial^2 p_s^{n+1}}{\partial x^2} + \frac{\partial^2 p_s^{n+1}}{\partial y^2}\right]_{ij} = \left[\frac{\varrho_0}{h}\int_0^h \left(\frac{\partial L(\bar{u}^{n+1}, \bar{v}^{n+1})}{\partial x} + \frac{\partial R^n}{\partial x} + \frac{\partial M(\bar{u}^{n+1}, \bar{v}^{n+1})}{\partial y} + \frac{\partial S^n}{\partial y}\right) d\zeta\right]_{ij}. \tag{25}$$

This set of equations is solved with the Neumann boundary condition. (The surface pressure is determined except for an additive constant, which is arbitrary, because only pressure gradients are used in the momentum equations).

Finally, the new horizontal velocity components u^{n+1} and v^{n+1} are derived from the right-hand sides of (21) and (22) by substituting p_s^n by p_s^{n+1}. The vertical velocity and the temperature are calculated from the discretized versions of (18) and (6) respectively, and $\hat{u}^n$ and $\hat{v}^n$ are calculated with (9). This completes the time step procedure.

3.3 Numerical stability

The finite difference scheme is such that the Coriolis terms conserve energy exactly (algebraically). Further, the new velocity-field satisfies exactly (algebraically) mass conservation equation (3). This desirable feature is also a property of the "Marker-and-Cell" method (MAC) from Harlow and Welch (1966). However, in the MAC scheme Coriolis and vertical diffusion are not treated implicitly.

Coriolis and vertical diffusion are treated implicitly in SOMS to avoid undesirable time step limits when the boundary layers are adequately resolved. Ekman layer thickness is roughly determined by scale analysis of a balance between vertical diffusion and Coriolis terms (Pedlovsky, 1984). If this thickness is adequately resolved, the smallest resolved vertical modes decay on a time scale that is small compared to the Coriolis time scale, leading to a generally undesirable time step limitation if the vertical diffusion is treated explicitly.

The main time step limiting processes are thus internal wave propagation, and horizontal advection and diffusion. Compared to internal wave terms, horizontal diffusion and advection are quite often relatively small.

4. Application of the model to Lake Neuchâtel

4.1 Description of the Lake

Lake Neuchâtel is a quasi-rectangular body of water in western Switzerland. Its surface is artificialy maintained at a mean altitude of 429 m above see-level by a dam. Its longest axis is directed SW-NE. The maximum length is 38.3 km, the average width 5.68 km, and the maximum depth 136 m. The bathymetry of the lake is "elongated bath-tub" like with a bump centered in the NE region (see fig. 2). This bump (ealled la Motte) is a rather steep mountain with its peak only about 10 m under the water-surface.

The dominant wind is le Vent, a SW wind, blowing along the long axis of the Lake.

More information about the morphology of the Lake, its inlets and its wind is found in Bapst (1988) and Sollberger (1974).

4.2 Simulation

The simulations performed were intended to provide a first overview of the general circulation in Lake Neuchâtel under barotropic conditions induced by the most prevailing wind.

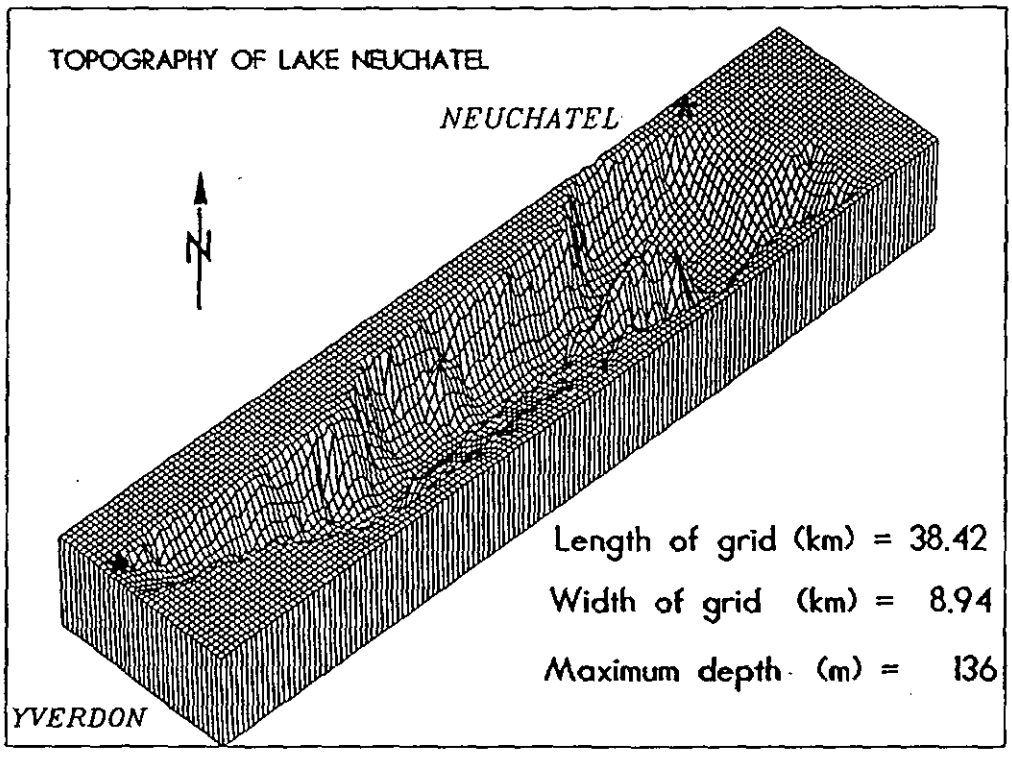

Figure 2. Topography of Lake Neuchâtel

The lake is considered to be a closed basin. So, the influence on the general circulation of rivers and small streams that enter the lake is neglected. The wind conditions are as follows. Wind is blowing from the south-west (le Vent). The wind speed remains constant the first twelve hours. Then the wind is turned off, and the model is kept running without wind-forcing for another six hours. At the start of both simulations the lake is at rest ($v = 0$).

The volume of the Lake is filled with control volumes. A horizontal plane contains 134×34 control volumes, the area of each control volume being 263×263 m^2. In the vertical direction there are 20 layers of control volumes, the thickness of each layer being defined by a vertically stretched vertical coordinate to model correctly the surface Ekman layer. The bottom Ekman layer is not resolved by the model, and therefore, instead of the no-slip condition, a shear stress law is applied at the bottom (see below).

The wind stress is related to the wind speed by a "bulk aerodynamic" formula

$$(\tau_{sx}, \tau_{sy}) = \varrho_a C_D \sqrt{(U^2 + V^2)}\,(U, V), \tag{26}$$

where ϱ_a ($= 1.225$ kg/m^3) is the air's density, $(U, V) = (7.5, 0)$ m/s is the air velocity at an elevation of 3 m above the lake-surface, and C_D ($= 0.002$) is the drag coefficient corresponding to this elevation. So, the boundary conditions for the velocity components at the surface are

$$\varrho_0 A_v \left(\frac{\partial u}{\partial z}, \frac{\partial v}{\partial z}\right) = (\tau_{sx}, \tau_{sy}), \tag{27}$$

$$w = 0. \tag{28}$$

The bottom shear stress is related to the velocity in the bottom layer according to

$$(\tau_{bx}, \tau_{by}) = \varrho_0 r \sqrt{(u_b^2 + v_b^2)}\,(u_b, v_b), \tag{29}$$

in which (u_b, v_b) is the horizontal velocity in the last layer. r ($= 0.0025$) is the drag coefficient at the bottom. The boundary conditions at the bottom are

$$\varrho_0 A_v \left(\frac{\partial u}{\partial z}, \frac{\partial v}{\partial z}\right) = (\tau_{bx}, \tau_{by}), \tag{30}$$

$$w = 0. \tag{31}$$

The horizontal turbulent viscosity coefficient is taken constant, $A_h = 10$ m^2/s. The vertical turbulent viscosity A_v is defined as (see Hutter, 1984)

$$A_v = \nu_0 + \nu_1 \sqrt{(\tau_{sx}^2 + \tau_{sy}^2)}\, e^{-z/d}, \tag{32}$$

in which $\nu_0 = 25$ cm^2/s, $\nu_1 = 100$ cm^3 s/gr, and $d = 20$ m.

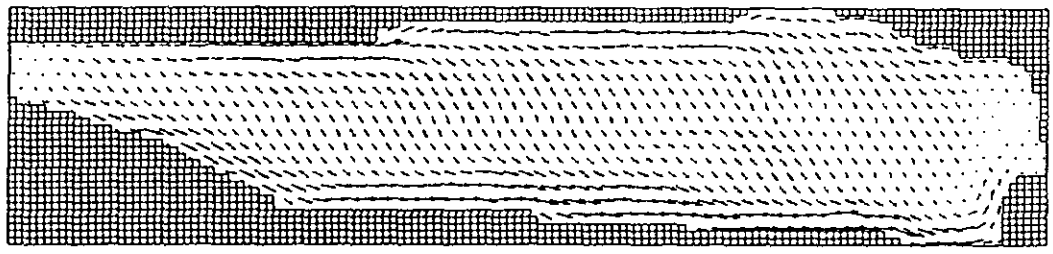

K= 1 Depth (m)= 0.30 VMAX (cm/s)= 31.76

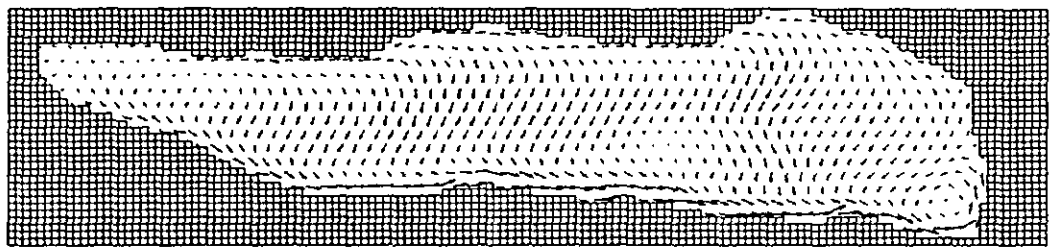

K= 5 Depth (m)= 11.80 VMAX (cm/s)= 17.95

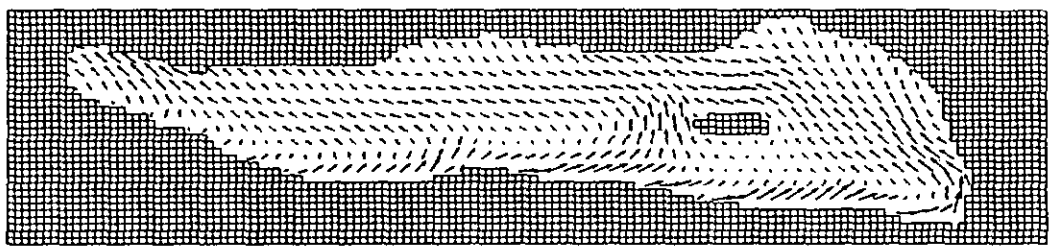

K= 9 Depth (m)= 34.20 VMAX (cm/s)= 8.53

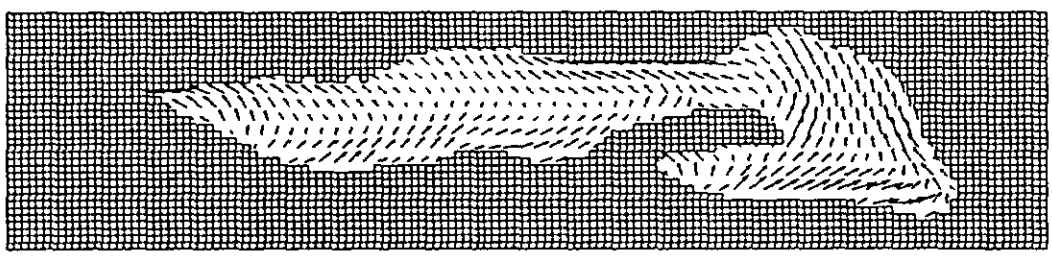

K= 13 Depth (m)= 65.00 VMAX (cm/s)= 5.35

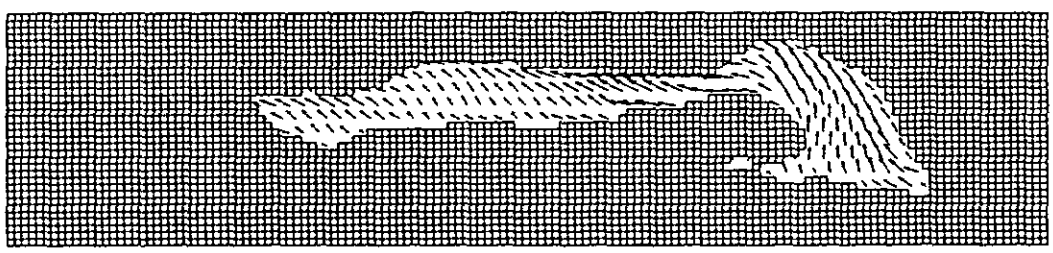

K= 17 Depth (m)= 103.00 VMAX (cm/s)= 4.72

Figure 3. Horizontal velocity field at 5 depth-levels after 12 hours of wind-forcing

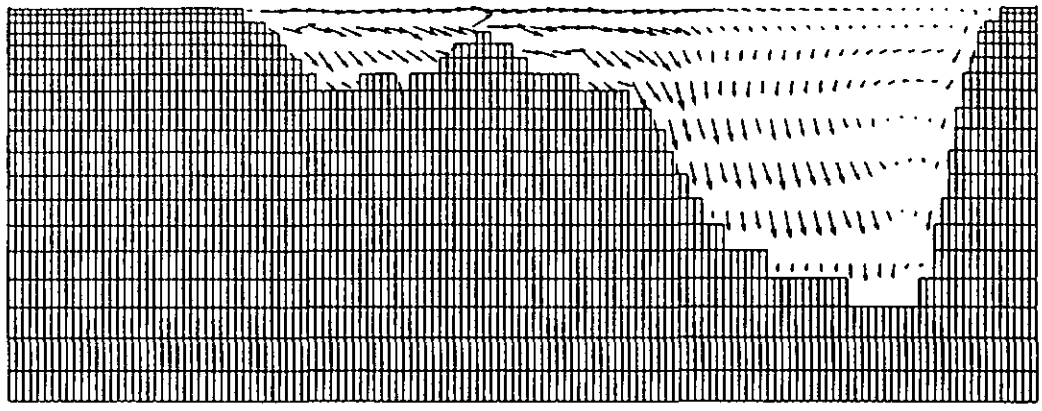

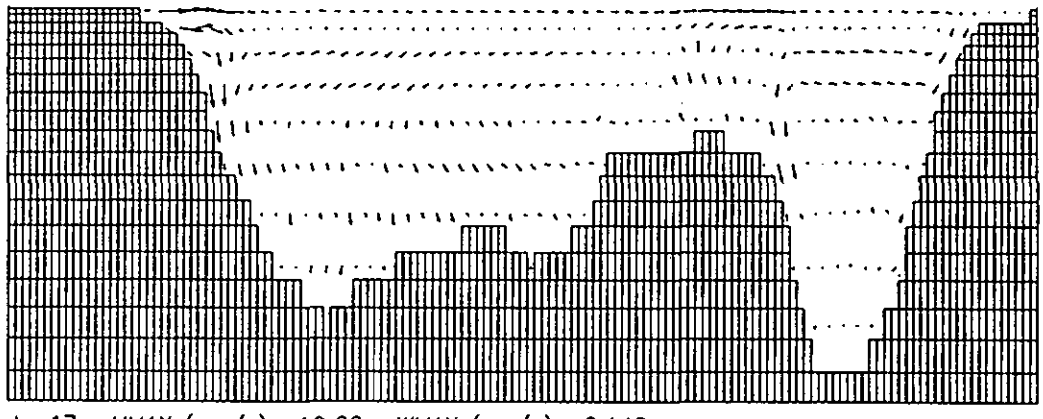

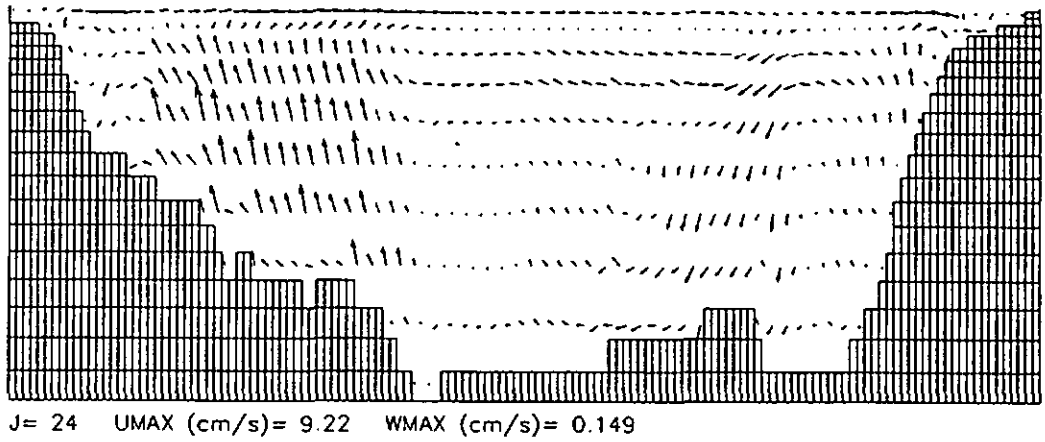

Figure 4. Velocity profiles in 3 longitudinal sections after 12 hours of wind-forcing. "J" increases from south-east to north-west

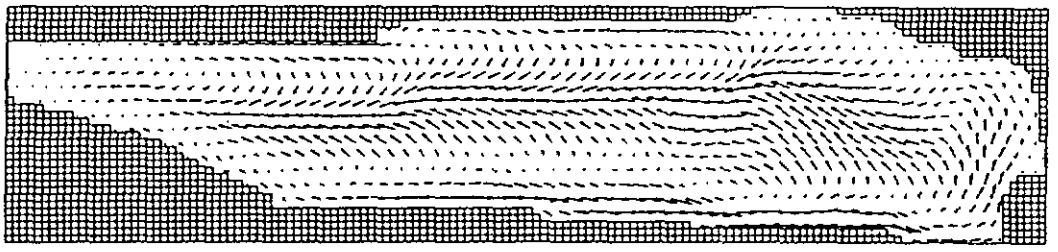

K= 1 Depth (m)= 0.30 VMAX (cm/s)= 12.01

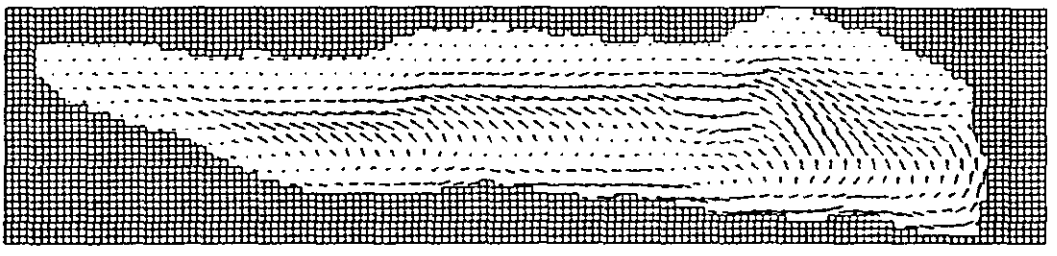

K= 5 Depth (m)= 11.80 VMAX (cm/s)= 9.58

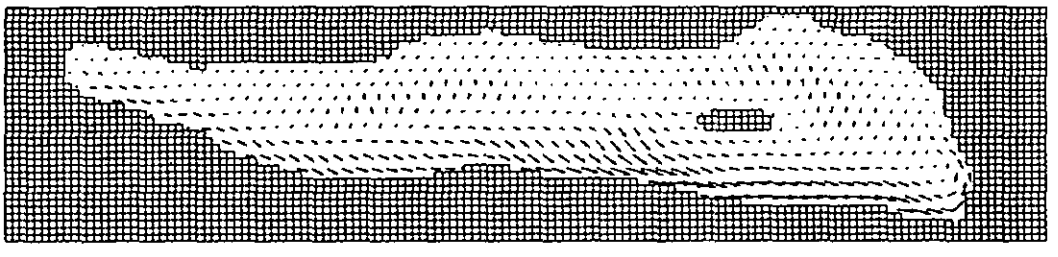

K= 9 Depth (m)= 34.20 VMAX (cm/s)= 7.83

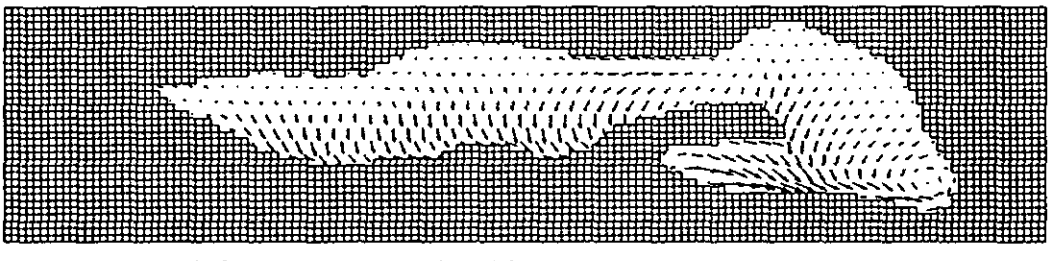

K= 13 Depth (m)= 65.00 VMAX (cm/s)= 4.63

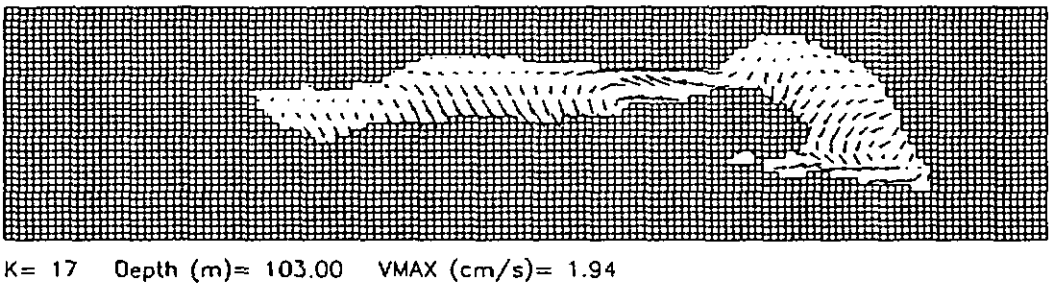

K= 17 Depth (m)= 103.00 VMAX (cm/s)= 1.94

Figure 5. Horizontal velocity field at 5 depth-levels after 18 hours, 6 hours after wind-forcing was stopped

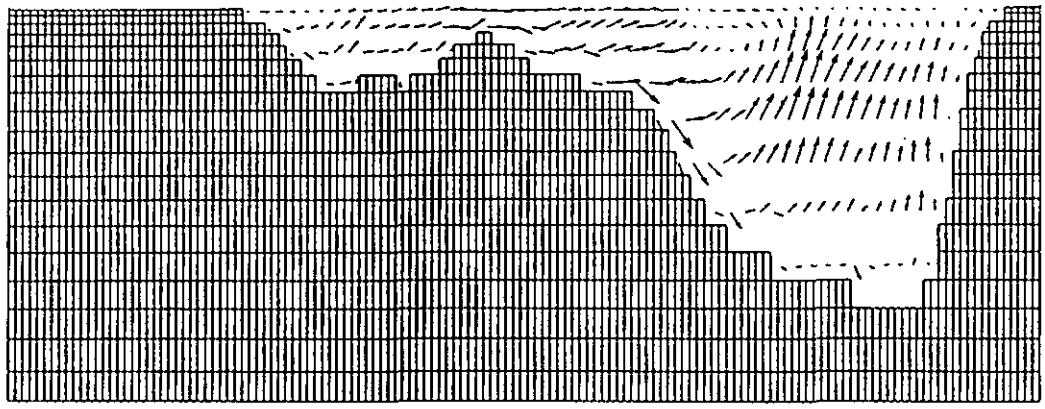

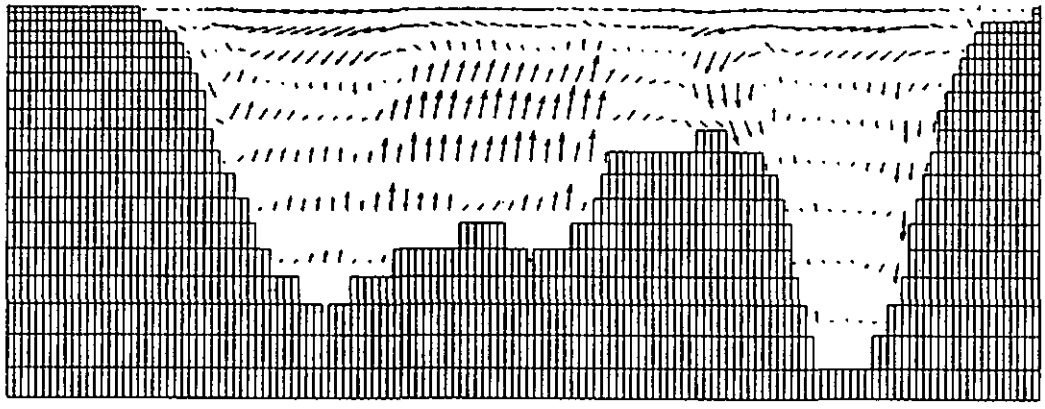

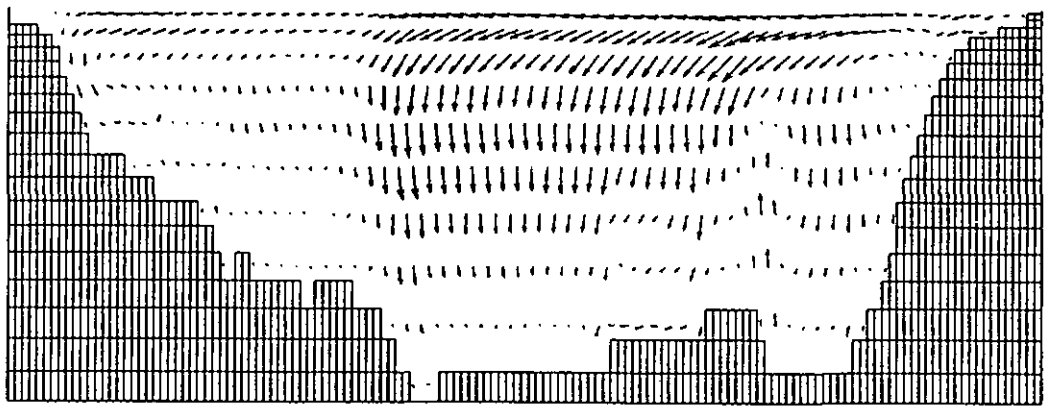

Figure 6. Velocity profiles in 3 longitudinal sections after 18 hours, 6 hours after wind-forcing was stopped. "J" increases from south-east to north-west

Other parameters used in the calculations have the following values:

- reference density: $\varrho_0 = 1000\ \mathrm{kg/m^3}$;
- Coriolis parameter: $f = 1.05 \times 10^{-4}\ \mathrm{s^{-1}}$;
- gravitational acceleration: $g = 9.8\ \mathrm{m/s^2}$;
- weight coeff. in FLTW method: $\omega = 0.1$;
- time step: $\Delta t = 60\ \mathrm{s}$.

4.3 Results

Results are presented in fig. 3 to fig. 6. For brevity, only 5 among the 20 depth-levels, and 3 among the 34 vertical slices in the length direction of the lake are diplayed. The size of the arrows is scaled according to the maximum velocity that occurs at that level/slice. So, the length of the longest vector at each level/slice is the same, and its magnitude is denoted under the corresponding plot. In the captions of the plots "K" and "J" denote the number of the depth-level and the cross-section respectively. "K" increases from top to bottom from 1 to 20, and "J" increases from south-east to north-west from 1 to 34. Figure 3 and fig. 4 show the situation after 12 hours, fig. 5 and fig. 6 after 18 hours.

After 12 hours of wind forcing the circulation is stationary. Near the surface away from the boundary the velocity-field is deflected to the right relative to the south-west wind (see fig. 3). The angle of this deflection agrees well with the theoretical value, being 45°, which is the limiting angle in the Ekman layer when the surface is approached (Pedlosky, 1986). As the net horizontal flow near the surface is directed east, it induces upwelling in the west- and downwelling in the east-part of the lake (see fig. 4). So, a vortex in the vertical west-east plane has been set up by the wind. After 12 hours the wind is turned off, and the vortex will start to propagate clockwise as to conserve vorticity (apart from the fact that energy is dissipated by eddy viscosity). The strong influence of the pronounced topography on the circulation makes it difficult to identify the mentioned vortex after 18 hours in the plots (see fig. 6). Away from the boundary in the middle of the lake the Coriolis force tends to rotate the velocity field horizontally with inertial period $2\pi/f \simeq 16.6$ hr, while the direction of the currents near the longside boundaries remains unchanged. As a result after 6 hours without wind-forcing two cells are formed in the upper layers, turning in opposite directions (see fig. 5).

5. Conclusions

The favourable stability characteristics of the SOMS model are due to the specific features of the numerical scheme, under which the facts that the mass conservation equation is satisfied in every cell at the end of every timestep, and the finite difference scheme is such that the Coriolis terms conserve energy exactly in the algebraic sense. Compared to explicit "free surface" models, the time step that can be taken in SOMS is much bigger as a result of the rigid lid approximation and the coupled implicit treatment of Coriolis and vertical diffusion.

Some results of applying the model to Lake Neuchâtel under barotropic conditions were presented. The phenomenological magnitudes in the model are the horizontal and vertical turbulent viscosity and the drag coefficients at the surface and bottom. As we had no relevant data available to determine these magnitudes experimentally, we took values which were determined for lakes with comparable dimensions. Since these magnitudes depend particularly on the considered length-scale, this approach is justified. In the near future an extensive field campaign will be carried out in Lake Neuchâtel. With the data that becomes available then, results from modelling the lake's circulation can be verified properly. Then SOMS will also be used to simulate the circulation under baroclinic conditions.

ACKNOWLEDGEMENTS

This research was performed within the framework of a collaboration between the PROSPER group (University of Neuchâtel, Switzerland) and Sandia National Laboratories (New Mexico). It was supported by the Swiss National Science Foundation (grant nr.: 2.055.086). The authors warmly thank Dr. François Nyffeler and Dr. Pat Roache for their contributions and guidance, and Dr. Melvin Marietta who promoted this collaborative effort.

REFERENCES

Arakawa, A., and V. R. Lamb, 1977. Computational design of the basic dynamical processes of the UCLA general circulation model. Methods in Computational Physics. 17:174–265.

Bapst, A., 1987. Le Lac de Neuchâtel: Thèse présentée a la Faculté des Sciences (Université de Neuchâtel).

Batchelor, G. K., 1967. An introduction to fluid dynamics. Cambridge University Press.

Dietrich, D. E., M. G. Marietta and P. J. Roache, 1987. An Ocean Modelling System with turbulent boundary layers and topography. International Journal for Numerical Methods in Fluids. 7:833–855.

Hutter, K., 1984. Mathematische Vorhersage von barotropen und baroklinen Prozessen im Zürich- und Luganersee. Vierteljahrschrift der Naturforschenden Gesellschaft in Zürich. 129:51–92.

Mellor, G. L., and T. Yamada, 1982. Development of a Turbulence Closure Model for Geophysical Fluid Problems. Reviews of geophysics and space physics. 20:851–875.

Pedlosky, J., 1987. Geophysical fluid dynamics. Springer, New York.

Roache, P. J., 1976. Computational Fluid Dynamics. Hermosa Publishers, Albuquerque, New Mexico.

Roache, P. J., and D. E. Dietrich, 1988. Evaluation of the filtered leapfrog-trapezoidal time integration method. Numerical Heat Transfer.

Sollberger, H., 1974. Le Lac de Neuchâtel: Thèse présentée a la Faculté des Sciences (Université de Neuchâtel).

Welch, J. E., F. H. Harlow, J. P. Shannon and B. P. Daly, 1966. The MAC Method, LA-3425. Los Alamos, New Mexico.

Received 20 December 1989;
revised manuscript accepted 16 January 1990.

THE PROSPER GENERAL CIRCULATION MODEL, AN ADAPTED FORM OF THE SANDIA OCEAN MODELLING METHOD: A NUMERICAL DESCRIPTION

E.A.H. Zuur

PROSPER, University of Neuchâtel (Switzerland)

SUMMARY

The PROSPER General Circulation Model (PGCM) is a three-dimensional model, based on the incompressible Navier-Stokes equations, an equation of state and the heat equation. The hydrostatic approximation and the rigid lid approximation are used. The system of equations is converted into an equivalent form, in which the surface pressure is more directly expressed in terms of a two-dimensional Poisson equation. The finite difference method is described and analysed. In particular the iteration method inside every time step to determine the new surface pressure and velocity components, and numerical diffusion aspects due to the use of the staggered Arakawa-C grid are looked at. Since part of the development of the PGCM code is a result of studying the Sandia Ocean Modelling System (SOMS), a comparison is made with respect to the concepts used in both models.

KEY WORDS Incompressible Flow Hydrostatic Approximation
Pressure Poisson Equation Staggered Grid
Numerical Diffusion

SHORT TITLE: THE PROSPER GENERAL CIRCULATION MODEL

1. INTRODUCTION

The starting-point for the PROSPER General Circulation Model (PGCM) that is discussed here, is the Sandia Ocean Modelling System (SOMS), developed by Dietrich, Marietta and Roache[1]. The performance of SOMS and a comparison with other models -in particular with respect to the Bryan-Semptner model[2,3]- in determining the large scale circulation in the North-Atlantic has been described by the authors here above[1]. An application in order to determine the general circulation in Lake Neuchatel (Switzerland) has been described by Zuur and Dietrich[4]. SOMS consists of two coupled models: the free-stream model, and a bottom boundary layer model to describe the turbulent processes in the boundary layer. In this paper, references made to SOMS relate only to the free-stream part.

A specific and important aspect of SOMS is the predictor-corrector method inside a time step to determine the new velocity components and surface pressure. In case of Neumann boundary conditions at the surface and bottom of the domain, the method used in PGCM is equivalent to the one used in SOMS. In case of Dirichlet conditions, however, in PGCM an extended form of the predictor-corrector method is used. Vertical diffusion is, like in SOMS, treated implicitly. In contrast with SOMS, in PGCM the Coriolis term is taken explicitly in the numerical scheme. Although explicit treatment of this term implies an a priori limitation by the Coriolis parameter for the time step, for lake circulations and mesoscale processes in the ocean the time step is not so much limited by this parameter, but by internal wave propagation and advection and horizontal diffusion terms. So, this disadvantage in comparison with SOMS is not relevant for these processes. The advantages of explicit treatment of the Coriolis term will become apparent in the remainder.

In this paper a description of the PGCM numerical algorithm

is presented. The iteration method inside a time step to determine the new velocity components and surface pressure is discussed in detail. Criteria for stability are derived. An analysis of numerical diffusion aspects in both the SOMS and the PGCM code is performed.

2. THE CONTINUUM EQUATIONS

2.1. The basic equations

The circulation model is based on the Navier-Stokes equations, written in the primitive variables. Scaling estimates of the terms that appear in these equations justify the following approximations that simplify the resulting system (Gill[5], Pedlosky[6]):

- The Bousinesq approximation: density variations are neglected in the horizontal momentum and mass conservation equations, but are included when they are associated with buoyancy forces (in the vertical momentum equation). Density is assumed independent of pressure and varies only with temperature.
- The hydrostatic approximation: all terms in the vertical momentum equation are negected except the buoyancy and pressure gradient terms.
- The rigid lid approximation.
- Turbulence is represented by means of horizontal and vertical turbulent viscosity coefficients.

The turbulent viscosity coefficients are taken constant. ρ is the normalized density (i.e. density divided by reference density). The kinematic pressure (i.e. pressure divided by reference density) is denoted by a capital P, in order to distinguish it from the kinematic surface pressure p, that will appear later on. The resulting continuum equations are stated below.

- The horizontal momentum equations:

$$u_t + \nabla.(u\vec{v}) - fv = - P_x + A_H\nabla_h^2 u + A_V u_{zz},$$

$$v_t + \nabla.(v\vec{v}) + fu = - P_y + A_H\nabla_h^2 v + A_V v_{zz}.$$

- The hydrostatic approximation equation:

$$P_z = \rho g$$

- The mass conservation equation:

$$u_x + v_y + w_z = 0.$$

- The equation of state:

$$\rho = (1 - \beta(T - T_o)).$$

- The heat equation

$$T_t + \nabla.(T\vec{v}) = K_H\nabla_h^2 T + K_V T_{zz}.$$

The above equations apply to a bounded domain Ω for t>0, subjected to Dirichlet or Neumann boundary conditions at $\partial\Omega$ for the horizontal velocity components and temperature. Due to the hydrostatic approximation second order spatial derivatives of the vertical velocity component w have disappeared. A consistent boundary condition for w is $w.n_3 = 0$, in which n_3 is the third component of the outward unit pointing normal $\vec{n} = (n_1, n_2, n_3)$ at the boundary $\partial\Omega$. The initial conditions are:

$$\vec{v}(x,0) = \vec{v}_o(x) \quad \text{in } \bar{\Omega} \equiv \Omega \cup \partial\Omega,$$

with

$$\nabla.\vec{v}_o = 0 \quad \text{in} \quad \Omega,$$

and

$$T(\vec{x},0) = T_o(\vec{x}) \quad \text{in} \quad \bar{\Omega}.$$

The following symbols are used:

x, y, z	spatial coordinates in a left-handed Cartesian system (z-axes points downwards) [L];
t	time [T];
T	temperature [Θ];
u, v, w	velocity components ($\vec{v} = (u,v,w)$) [LT^{-1}];
P	kinematic pressure [L^2T^2];
ρ	normalized density;
g	effective gravitational acceleration [LT^{-2}];
A_H, A_V, K_H, K_V	turbulent viscosity and diffusion coefficients [L^2T^{-1}];
f	Coriolis parameter [T^{-1}];
β	coefficient of thermal expansion [Θ^{-1}];
∇	$\equiv (\partial/\partial x, \partial/\partial y, \partial/\partial z)$;
∇_h^2	$\equiv \partial^2/\partial x^2 + \partial^2/\partial y^2$.

2.2. The equivalent formulation

Like the SOMS model, the PGCM model uses an equivalent form of the above set of equations, based on *the equivalence assertion for incompressible flows* as described by Gresho and Sani[7]. This assertion, although not formally proved by the authors, has been verified thouroughly in practice, among others by Abdallah and Dreyer[8]. We will assume its correctness. The assertion is used to convert the original set of equations into one in which the pressure is more directly expressed in terms of the so-called pressure Poisson equation, which is derived from the mass conservation and the momentum equations, and that will replace (together with an appropriate boundary condition) the mass conservation equation, giving the equivalent formulation of the problem. The assertion in its original form was stated with respect to the full incompressible Navier-Stokes equations. We apply the same ideas to the case in which the hydrostatic approximation is used.

Let us derive the equivalent formulation in the hydrostatic case. From the hydrostatic equation and the equation of state it follows that

$$P = p(x,y,t) + gz - g\beta\int_o^z T(x,y,\zeta,t)d\zeta,$$

in which p is the surface pressure (which is different from the atmospheric pressure due to the rigid lid approximation). Define the terms R and S, that are treated explicitly in the integration scheme:

$$R = g\beta\int_o^z T_x d\zeta - \nabla.(u\vec{v}) + fv + A_H\nabla_h^2 u,$$

$$S = g\beta\int_o^z T_y d\zeta - \nabla.(v\vec{v}) - fu + A_H\nabla_h^2 v.$$

With the above definitions the momentum equations take the form

$$u_t = - p_x + A_V u_{zz} + R,$$

$$v_t = - p_y + A_V v_{zz} + S.$$

Due to the rigid lid approximation, the vertical velocity is zero at the surface. The mass conservation equation yields

$$w = \int_o^z (u_x + v_y)d\zeta. \qquad (1)$$

Boundary condition $w.n_3 = 0$ at the bottom gives

$$0 = \int_o^h (u_x + v_y)d\zeta, \qquad (2)$$

in which $h = h(x,y)$ is the bottom-depth. By taking the horizontal

divergence of both sides of the momentum equations, integrating the result from surface to bottom (from (2) and the initial condition $\nabla.\vec{v}_o = 0$ it follows that the remaining left-hand side is zero), we obtain a two dimensional Poisson equation for the surface pressure

$$\nabla_h^2 p = \frac{1}{h}\int_0^h \{ \frac{\partial}{\partial x}[A_V u_{zz} + R] + \frac{\partial}{\partial y}[A_V v_{zz} + S]\}dz.$$

The correct boundary condition in the equivalent formulation for the pressure Poisson equation is a Neumann condition that is derived simply by applying the normal component of the momentum equations at the surface boundary $\partial\Omega_s$:

$$\frac{\partial p}{\partial \vec{n}_s} = \vec{n}_s.(A_V u_{zz} + R - u_t, A_V v_{zz} + S - v_t) \quad \text{at} \quad \partial\Omega_s,$$

in which $\vec{n}_s = (n_1, n_2)$ is the outward unit pointing normal at the boundary of the surface Ω_s.

Instead of the original problem, we consider from now on the equivalent problem in which the mass conservation equation is replaced by the pressure Poisson equation and the above boundary condition. The vertical velocity component w, appearing in the R and S terms, is in this new formulation by definition given by (1), and is therefore no longer considered as being an unknown.

Besson and Laydi[9] show that the solution of the original problem exists in some Sobolev-space. However, additional regularity requirements are implied by the 'equivalent' formulation. *Throughout this paper we will assume* u, v, p, *and* T *to be in* $C^2(\bar{\Omega})$ *for* $t \geq 0$, *in which* $C^2(\bar{\Omega})$ *is the set of functions having all spatial derivatives of order* ≤ 2 *continuous in* Ω, *with continuous extensions to* $\bar{\Omega}$.

3. THE NUMERICAL ALGORITHM

3.1. The time integration scheme

The time integration procedure is such that three time-levels are involved in every time-step: the time-level n+1 for which the velocity, pressure and temperarure have to be calculated, and the two time-levels n and n-1 for which the corresponding physical quantities are known from previous iterations. The choise of which terms are considered at time-level n+1, n, and n-1, respectively, will be justified in the next sections in which the spatial discretization and the stability of the scheme are discussed.

Using a centered difference discretization for the time-derivative operator, the time-integration problem for the momentum equations, the surface pressure Poisson equation and the heat equation reads as follows:

Given u^{n-1}, v^{n-1}, p^{n-1}, T^{n-1}, u^n, v^n, p^n, and T^n, find u^{n+1}, v^{n+1}, p^{n+1}, and T^{n+1}, such that

$$u^{n+1} = u^{n-1} + 2\Delta t[-p_x^{n+1} + A_v u_{zz}^{n+1} + R^n],$$

$$v^{n+1} = v^{n-1} + 2\Delta t[-p_y^{n+1} + A_v v_{zz}^{n+1} + S^n],$$

$$\nabla_h^2 p^{n+1} = \frac{1}{h}\int_0^h \left(\frac{\partial}{\partial x}[A_v u_{zz}^{n+1} + R^n] + \frac{\partial}{\partial y}[A_v v_{zz}^{n+1} + S^n]\right)dz,$$

$$T^{n+1} = T^{n-1} + 2\Delta t[-\nabla.(T^n \vec{v}^{n+1}) + K_H \nabla^2 T^{n-1} + K_v T_{zz}^{n+1}],$$

with

$$R^n = g\beta\int_o^z T_x^n d\zeta - \nabla.(u^n \vec{v}^n) + fv^n + A_H \nabla_h^2 u^{n-1},$$

and

$$S^n = g\beta\int_0^z T_y^n d\zeta - \nabla.(v^n\vec{v}^n) - fu^n + A_H\nabla_h^2 v^{n-1}.$$

The boundary conditions for u^{n+1} and v^{n+1} at the surface and bottom of the domain are either Dirichlet, Neumann or a mixture of both. Although the iteration procedure to solve the above system is valid for all sorts of linear combinations of these boundary conditions, to fix ideas, let us put a Neumann condition at the surface, expressing wind stress, and a Dirichlet condition at the bottom, expressing no-slip:

$$\frac{\partial u^{n+1}}{\partial z} = \sigma \quad \text{and} \quad \frac{\partial v^{n+1}}{\partial z} = \tau \quad \text{at } z = 0,$$

$$u^{n+1} = v^{n+1} = 0 \quad \text{at} \quad z = h.$$

The boundary condition for the surface pressure is

$$\frac{\partial p^{n+1}}{\partial \vec{n}_s} = \vec{n}_s.\vec{b}^n \quad \text{at } \partial\Omega_s,$$

with

$$\vec{b}^n = \left(A_V u_{zz}^n + R^n - \frac{u^n - u^{n-1}}{\Delta t}, A_V v_{zz}^n + S^n - \frac{v^n - v^{n-1}}{\Delta t}\right).$$

u^{n+1}, v^{n+1}, and p^{n+1} are determined using an iterative procedure. After these quantities are known the temperature is updated with the discretized heat equation in a straight-forward manner, and the time-step is completed. Define the following quantities

$$\alpha^z = (2\Delta t A_v)^{-1}, \quad \bar{p}^{n+1} = 2\Delta t p^{n+1},$$

$$\bar{u}^{n+1} = u^{n+1} + 2\Delta t p_x^{n+1}, \quad \bar{v}^{n+1} = v^{n+1} + 2\Delta t p_y^{n+1},$$

$$\bar{R}^n = u^{n-1} + 2\Delta t R, \quad \bar{S}^n = v^{n-1} + 2\Delta t S^n.$$

Let m denote the iteration parameter of the procedure. By using the identity

$$\int_0^h (u_x^{n-1} + v_y^{n-1}) dz = 0,$$

and by replacing the original quantities by the overbar quantities in the time-integration scheme, we obtain the following iteration procedure:

$$\bar{u}^{n+1,m+1} - \alpha^{-z} \bar{u}_{zz}^{n+1,m+1} = \bar{R}^n,$$

$$\bar{v}^{n+1,m+1} - \alpha^{-z} \bar{v}_{zz}^{n+1,m+1} = \bar{S}^n,$$

$$\nabla_h^z \bar{p}^{n+1,m+1} = \frac{1}{h} \int_0^h (\bar{u}_x^{n+1,m+1} + \bar{v}_y^{n+1,m+1}) dz,$$

with boundary conditions

$$\frac{\partial \bar{u}^{n+1,m+1}}{\partial z} = \alpha, \quad \frac{\partial \bar{v}^{n+1,m+1}}{\partial z} = \tau \quad \text{at} \quad z = 0,$$

$$\bar{u}^{n+1,m+1} = -\bar{p}_x^{n+1,m}, \quad \bar{v}^{n+1,m+1} = -\bar{p}_y^{n+1,m} \quad \text{at} \quad z = h.$$

$$\frac{\partial \bar{p}^{n+1,m+1}}{\partial \vec{n}_s} = 2\Delta t \vec{n}_s \cdot \vec{b}^n \quad \text{at } \partial\Omega_s.$$

The procedure is initialized with any start value for $\bar{p}^{n+1,0}$ (for

example $\bar{p}^{n+1,0} = 2\Delta t p^n$). Notice, that in the 'overbar system' the pressure gradient terms no longer occur in the first two equations, but instead in the corresponding Dirichlet boundary conditions. Successive iterations are coupled only through these terms, i.e. through $\bar{p}_x^{n+1,m}$ and $\bar{p}_y^{n+1,m}$. In case both the surface and the bottom boundary conditions are Neumann, there is no coupling and the system is solved in one iteration only. Then we get

$$p^{n+1} = \frac{1}{2\Delta t}\bar{p}^{n+1,1},$$

$$u^{n+1} = \bar{u}^{n+1,1} - 2\Delta t p_x^{n+1}, \quad \text{and} \quad v^{n+1} = \bar{v}^{n+1,1} - 2\Delta t p_y^{n+1}.$$

In this case the method is equivalent to the predictor-corrector method used in SOMS (apart from the explicit treatment of the Coriolis terms). In case of Dirichlet conditions at the surface and/or bottom, in general more iterations are required to approximate $\bar{u}^{n+1}$, $\bar{v}^{n+1}$ and $\bar{p}^{n+1}$ properly. The condition for convergence of the procedure is derived in section 4.1. Assuming this condition is satisfied we formally have

$$(\bar{u}^{n+1}, \bar{v}^{n+1}, \bar{p}^{n+1}) = \lim_{m\to\infty} (\bar{u}^{n+1,m}, \bar{v}^{n+1,m}, \bar{p}^{n+1,m}).$$

All three equations in the iteration scheme are decoupled, and are evaluated one after another. The first two equations are solved either directly or with a relaxation method. Since the unknowns $\bar{u}^{n+1,m+1}$ and $\bar{v}^{n+1,m+1}$ only have derivatives to z, the equations can be evaluated at successive horizontal positions. The two dimensional Poisson equation that determines $\bar{p}^{n+1,m+1}$ is solved using a SOR method, or a fast marching method for elliptic problems such as developed by Dietrich *et al.*[10] and Roache[11].

3.2. The finite differences in space

Spatial discretization is based on the concept of control volumes (Roache[12]). The control volume approach to deriving finite

difference equations relates the time derivatives of volume-integrated conserved quantity densities in each control volume to corresponding fluxes integrated over the boundaries of the control volume. The bounded domain Ω is discretized into a finite number of cubical control volumes. The grid is regular, but stretched in the vertical coordinate, in order to model accurately the surface and/or bottom boundary layer. The control volumes for the different physical quantities are actually staggered in space, corresponding to the Arakawa-C grid from Arakawa and Lamb[13] (see fig.1). In this grid four different types of control volumes are distinguised: the P-cells for pressure, and the U-, V-, and W-cells for the respective velocity components. Control volumes for any scalar quantity, such as temperature, coincide with the P-cells. The P-cells are considered to be either wholly inside or wholly outside Ω.

Let us derive the finite difference formulation for the heat equation to illustrate the above approach. Rewrite the heat equation in the form

$$T_t + \nabla.\vec{F} = 0,$$

in which

$$\vec{F} = (uT - K_H T_x,\ vT - K_H T_y,\ wT - K_V T_z),$$

is the flux density vector. Now consider the flux through the right side of the P-cell i,j,k. The finite difference formulation of the flux through this side per unit time per unit area is given by:

$$F_1(i+1/2,j,k) = u^n_{i,j,k}(T^n_{i+1,j,k} + T^n_{i,j,k})/2 - K_H \frac{T^{n-1}_{i+1,j,k} - T^{n-1}_{i,j,k}}{\Delta x}.$$

Discretization of the fluxes through the other sides of the control volume is analogous, except for the implicit treatment of the vertical diffusion term in the third component of the flux density vector. The change in temperature is now calculated from

the sum of the fluxes over the sides of the volume element, giving the finite difference analog of the heat equation

$$\frac{T^{n+1}_{i,k} + T^{n-1}_{i,k}}{2\Delta t} + U\frac{T^{n}_{i+1,k} - T^{n}_{i-1,k}}{2\Delta x} + W\frac{T^{n}_{i,k+1} + T^{n}_{i,k-1}}{2\Delta z} = \tag{3}$$

$$K_H\frac{T^{n-1}_{i+1,k} - 2T^{n-1}_{i,k} + T^{n-1}_{i-1,k}}{\Delta x^2} + K_V\frac{T^{n+1}_{i,k+1} - 2T^{n+1}_{i,k} + T^{n+1}_{i,k-1}}{\Delta z^2},$$

in which the y-component has been suppressed and the advection velocity is taken constant, in order to keep the expression conveniently arranged. It is observed, that the finite difference formulation for the heat equation is basically a combination of the leapfrog method for the advection terms, the forward differencing method for the horizontal diffusion terms, and implicit treatment of the vertical diffusion term.

The corresponding terms in the momentum equations are treated in exactly the same manner as in the heat equation. However, the first momentum equation is evaluated with respect to the U-cells, and the second with respect to the V-cells.

4. ANALYSIS OF THE ALGORITHM

4.1 Convergence of the iteration procedure

Consider the iteration procedure inside a time step defined in section 3.1. By suppressing the time step superscript we get

$$\bar{u}^{m+1} - \alpha^{-2}\,\bar{u}^{m+1}_{zz} = \bar{R},$$

$$\bar{v}^{m+1} - \alpha^{-2}\,\bar{v}^{m+1}_{zz} = \bar{S},$$

$$\nabla_h^2 \bar{p}^{m+1} = \frac{1}{h} \int_0^h (\bar{u}_x^{m+1} + \bar{v}_y^{m+1}) dz,$$

with boundary conditions

$$\frac{\partial \bar{u}^{m+1}}{\partial z} = \sigma, \qquad \frac{\partial \bar{v}^{m+1}}{\partial z} = \tau \quad \text{at} \quad z = 0,$$

$$\bar{u}^{m+1} = -\bar{p}_x^m, \quad \bar{v}^{m+1} = -\bar{p}_y^m \quad \text{at} \quad z = h.$$

$$\frac{\partial \bar{p}^{m+1}}{\partial \vec{n}_s} = 2\Delta t \vec{n}_s . \vec{b}^n \quad \text{at } \partial\Omega_s .$$

Let $\bar{p}^0$ be any given start value. Although $\bar{u}^0$ and $\bar{v}^0$ are not defined by the procedure, we introduce them artificially and set $\bar{u}^0 = \bar{v}^0 = 0$. First $\bar{u}^1$, $\bar{v}^1$ and $\bar{p}^1$ are determined from the above equations. Define

$$d^m = \bar{u}^m - \bar{u}^{m-1}, \; e^m = \bar{v}^m - \bar{v}^{m-1}, \; q^m = \bar{p}^m - \bar{p}^{m-1}, \text{ for } m = 1,2...$$

Notice that $d^1 = \bar{u}^1$, $e^1 = \bar{v}^1$ and $q^1 = \bar{p}^1 - \bar{p}^0$. For $m = 1,2...$ we obtain the following system for the differences:

$$d^{m+1} - \alpha^{-2} d_{zz}^{m+1} = 0,$$

$$e^{m+1} - \alpha^{-2} e_{zz}^{m+1} = 0,$$

$$\nabla_h^2 q^{m+1} = \frac{1}{h} \int_0^h (d_x^{m+1} + e_y^{m+1}) dz,$$

with boundary conditions

$$\frac{\partial d^{m+1}}{\partial z} = 0, \qquad \frac{\partial e^{m+1}}{\partial z} = 0 \quad \text{at} \quad z = 0,$$

$$d^{m+1} = - q_x^m, \quad e^{m+1} = - q_y^m \quad \text{at} \quad z = h,$$

$$\frac{\partial q^{m+1}}{\partial \vec{n}_s} = 0 \quad \text{at } \partial\Omega_s .$$

From the first two equations and the corresponding boundary conditions it follows that

$$d^{m+1} = - q_x^m \frac{\cosh(\alpha z)}{\cosh(\alpha h)}, \qquad e^{m+1} = - q_y^m \frac{\cosh(\alpha z)}{\cosh(\alpha h)}.$$

Taking the horizontal divergence $\nabla_h.(d^{m+1},e^{m+1})$ of the above expressions, and putting the result in the Poisson equation yields

$$\nabla_h^2 q^{m+1} = \frac{-1}{\alpha h} \tanh(\alpha h)[\nabla_h^2 q^m + \alpha(\nabla_h q^m).(\nabla_h h)\tanh(\alpha h)].$$

Let $|.|_\infty$ be the supremum norm defined on Ω_s. Since $\partial q^m/\partial \vec{n}_s = 0$ at $\partial\Omega_s$, we have

$$|\nabla_h q^m|_\infty \le C|\nabla_h^2 q^m|_\infty,$$

in which C is a constant determined by the dimension of Ω_s. Assuming that h is sufficiently regular, define

$$\omega = \left|\frac{\tanh(\alpha h)}{\alpha h}\right|_\infty + C\left|\tanh^2(\alpha h)\frac{\nabla_h h}{h}\right|_\infty .$$

We find

$$|\nabla_h q^{m+1}|_\infty \le C|\nabla_h^2 q^{m+1}|_\infty \le C\omega|\nabla_h^2 q^m|_\infty \le C\omega^m|\nabla_h^2 q^1|_\infty .$$

For $\omega < 1$ the method converges. Since we have put $\bar{u}^o = \bar{v}^o = 0$ we

get

$$\bar{u} = \sum_{m=1}^{\infty} d^m, \qquad \bar{v} = \sum_{m=1}^{\infty} e^m.$$

In case both the surface and the bottom boundary conditions are Dirichlet, a similar condition as above can be derived. We then get the condition

$$2\left|\frac{\cosh(\alpha h) - 1}{\alpha h \sinh(\alpha h)}\right|_\infty + C\left|\left(\frac{\cosh(\alpha h) - 1}{\sinh(\alpha h)}\right)^2 \frac{\nabla_h h}{h}\right|_\infty < 1.$$

In all but extreme cases with very pronounced topography, both conditions are always fulfilled.

4.2. Stability

Although we do not derive a rigorous stability criterium that applies to the entire integration scheme, by considering the separate terms of interest, limitations for the time step are derived, that in general are sufficient to assure stability of the method.

In order to derive the time step limitation due to the explicit treatment of the Coriolis term, consider only the corresponding part in the iteration scheme

$$u_{i,j}^{n+1} = u_{i,j}^{n-1} + 2\Delta t f \tfrac{1}{4}(v_{i,j}^{n} + v_{i+1,j}^{n} + v_{i,j-1}^{n} + v_{i+1,j-1}^{n}),$$

$$v_{i,j}^{n+1} = v_{i,j}^{n-1} - 2\Delta t f \tfrac{1}{4}(u_{i,j}^{n} + u_{i,j+1}^{n} + u_{i-1,j}^{n} + u_{i-1,j+1}^{n}),$$

in which the first equation is evaluated in the U-cells and the second in the V-cells. Notice, that the velocity components in the Coriolis terms are interpolated to these cells. These interpolation are justified in the next section. Let $\hat{u}$ and $\hat{v}$ denote the spatial Fourier transforms of the velocity components u

and v, respectively. Taking the Fourier transform of the above equations yields

$$\hat{u}^{n+1} = \hat{u}^{n-1} + \gamma\,\hat{v}^{n},$$

$$\hat{v}^{n+1} = \hat{v}^{n-1} - \bar{\gamma}\,\hat{u}^{n},$$

with

$$\gamma = \tfrac{1}{2}\Delta t f[1 + e^{-i\xi} + e^{i\vartheta} + e^{-i\xi}e^{i\vartheta}],$$

in which ξ and ϑ are the phase angles of the Fourier components in the x- and y-coordinate respectively, and $\bar{\gamma}$ is the complex conjugate of γ. Define $\hat{r}^{n+1} = \hat{u}^{n}$, and $\hat{s}^{n+1} = \hat{v}^{n}$. With these definitions the above system can be written as

$$\begin{pmatrix} \hat{u}^{n+1} \\ \hat{v}^{n+1} \\ \hat{r}^{n+1} \\ \hat{s}^{n+1} \end{pmatrix} = \begin{pmatrix} 0 & \gamma & 1 & 0 \\ -\bar{\gamma} & 0 & 0 & 1 \\ 1 & 0 & 0 & 0 \\ 0 & 1 & 0 & 0 \end{pmatrix} \begin{pmatrix} \hat{u}^{n} \\ \hat{v}^{n} \\ \hat{r}^{n} \\ \hat{s}^{n} \end{pmatrix}.$$

A necessary and sufficient condition for the above scheme to be stable is that the norm of the above matrix S is smaller or equal to one, i.e $||S|| \leq 1$. By determining the eigenvalues of S, it is readily verified that this is the case if $|\gamma| \leq 2$. The corresponding limitation for Δt follows from the definition of γ:

$$\Delta t \leq 1/f.$$

In a similar fashion a criterium for stability is derived with respect to the advection and diffusion terms by taking the Fourier transform of the discretized heat equation (4). The resulting condition for stability is

$$\left(\frac{|U|}{\Delta x} + \frac{|V|}{\Delta y} + \frac{|W|}{\Delta z}\right)^2 \Delta t^2 + 4K_H\left(\frac{1}{\Delta x^2} + \frac{1}{\Delta y^2}\right)\Delta t \leq 1, \qquad (5)$$

in which U, V and W should be interpreted as the maximum

velocities that occur in Ω. Since the corresponding terms in the momentum equations are treated in exactly the same manner, the same type of restriction can be derived for these equations. Then, in the above expression K_H is replaced by A_h.

The rigid-lid boundary condition eliminates the highest frequency surface wave components. However, it is mentioned that high-frequency internal waves can still limit the time step.

4.3. Numerical diffusion in SOMS and PGCM

By considering the integration of the Coriolis terms in the momentum equations, diffusive aspects in SOMS and PGCM are studied as a result of interpolating physical quantities to different control volumes of the Arakawa-C grid. In order to study the effect of these interpolations, we will look at the difference between the velocities obtained by the actual algorithms, and the velocities that would have been obtained when no interpolations of quantities would have been necessary to approximate them with respect to different control volumes.

In SOMS the Coriolis terms are treated implicitly. Therefore, the non-interpolated scheme reads as follows

$$u_{i,j}^{n+1} = u_{i,j}^{n-1} + 2\Delta t f v_{i+1/2,j-1/2}^{n+1}$$

$$v_{i,j}^{n+1} = v_{i,j}^{n-1} - 2\Delta t f u_{i-1/2,j+1/2}^{n+1}$$

The above equations are coupled through the implicit terms, and both equations relate to different types of cells, the U- and V-cells respectively. In order to solve the above system, in SOMS both equations are first interpolated to the P-cells, and the new velocity components are computed with respect to these cells. The interpolated scheme is

$$\tilde{u}^{n+1}_{i-1/2,j} = \frac{1}{2}(u^{n-1}_{i,j} + u^{n-1}_{i-1,j}) + 2\Delta t f \tilde{v}^{n+1}_{i,j-1/2},$$

$$\tilde{v}^{n+1}_{i,j-1/2} = \frac{1}{2}(v^{n-1}_{i,j} + v^{n-1}_{i,j-1}) - 2\Delta t f \tilde{u}^{n+1}_{i-1/2,j},$$

in which a tilde (~) denotes a quantity obtained with the actual algorithm. After the above system is solved the new velocity components are interpolated back to their respective cells to complete the procedure:

$$\tilde{u}^{n+1}_{i,j} = \frac{1}{2}(\tilde{u}^{n+1}_{i-1/2,j} + \tilde{u}^{n+1}_{i+1/2,j}),$$

$$\tilde{v}^{n+1}_{i,j} = \frac{1}{2}(\tilde{v}^{n+1}_{i,j-1/2} + \tilde{v}^{n+1}_{i,j+1/2}).$$

Consider the difference between $\tilde{u}_{i,j}$ and $u_{i,j}$. With the above equalities the difference can be expressed as

$$\tilde{u}^{n+1}_{i,j} - u^{n+1}_{i,j} = \frac{\Delta x^2}{4}\frac{u^{n-1}_{i+1,j} - 2u^{n-1}_{i,j} + u^{n-1}_{i-1,j}}{\Delta x^2} +$$

$$+ \Delta t f \frac{\Delta x^2}{4}\left[\frac{v^{n-1}_{i+1,j-1/2} - 2v^{n-1}_{i+1/2,j-1/2} + v^{n-1}_{i,j-1/2}}{(\Delta x/2)^2}\right] +$$

$$+ \Delta t f \frac{\Delta y^2}{8}\left[\frac{v^{n-1}_{i,j} - 2v^{n-1}_{i,j-1/2} + v^{n-1}_{i,j-1}}{(\Delta y/2)^2} + \frac{v^{n-1}_{i+1,j} - 2v^{n-1}_{i+1,j-1/2} + v^{n-1}_{i+1,j-1}}{(\Delta y/2)^2}\right] +$$

$$- 4\Delta t^2 f \frac{v^{n+1}_{i+1/2,j-1/2} - v^{n-1}_{i+1/2,j-1/2}}{2\Delta t} - 2(\Delta t f)^2(\tilde{u}^{n+1}_{i+1/2,j} + \tilde{u}^{n+1}_{i-1/2,j}).$$

Let U be the maximum velocity that occurs in Ω, and L be a charateristic length scale. The characteritic time interval of interest is $T = f^{-1}$. Assume $\Delta x \geq \Delta y$. The orders of magnitude of

the respective terms on the right hand side are for the first term $O(U\Delta x^2/L^2)$, for the second and third $O(U\Delta tf\Delta x^2/L^2)$, and for the fourth and fifth $O(U(\Delta tf)^2)$. Assuming $\Delta tf < 1$, the dominant term is the first one. This term expresses pure numerical diffusion over the time interval Δt. So, the numerical diffusion A_N per time unit is

$$A_N = \frac{\Delta x^2}{4\Delta t}.$$

A_N is considerable. As a matter of fact it is even more than the maximum tolerable physical horizontal diffusion in PGCM on account of the stability analysis (5) performed in section 4.2. Further, if Δt gets smaller, A_N gets bigger, which is disadvantageous if Δt is restricted by advection or internal wave terms.

It is mentioned that the authors of the SOMS model were aware of dispersive errors due to the implicit treatment of the Coriolis terms. However, they prefered their method to explicit treatment for reasons that relate to the coupling of the free-stream part with the bottom boundary layer part of their model (Dietrich *et al.*[1]).

In the PGCM scheme Coriolis is treated explicitly, and the momentum equations are evaluated in their respective U- and V-cells. The non-interpolated scheme is

$$u^{n+1}_{i,j} = u^{n-1}_{i,j} + 2\Delta tf v^{n}_{i+1/2,j-1/2},$$

$$v^{n+1}_{i,j} = v^{n-1}_{i,j} - 2\Delta tf u^{n}_{i-1/2,j+1/2}.$$

Consider the first equation. $v^n_{i+1/2,j-1/2}$ is approximated by

$$\tilde{v}^n_{i+1/2,j-1/2} = \frac{1}{4}\,(v^n_{i,j} + v^n_{i+1,j} + v^n_{i+1,j-1} + v^n_{i,j-1}),$$

and we solve

$$\tilde{u}^{n+1}_{i,j} = u^{n-1}_{i,j} + 2\Delta t f \tilde{v}^{n}_{i+1/2,j-1/2},$$

The difference between $\tilde{u}^{n+1}$ and u^{n+1} is

$$\tilde{u}^{n+1}_{i,j} - u^{n+1}_{i,j} = 2\Delta t f(\tilde{v}^{n}_{i+1/2,j-1/2} - \tilde{v}^{n}_{i+1/2,j-1/2}) =$$

$$+ \Delta t f \frac{\Delta x^2}{8}\left[\frac{v^n_{i+1,j} - 2v^n_{i+1/2,j} + v^n_{i,j}}{(\Delta x/2)^2} + \frac{v^n_{i+1,j-1} - 2v^n_{i+1/2,j-1} + v^n_{i,j-1}}{(\Delta x/2)^2}\right] +$$

$$+ \Delta t f \frac{\Delta y^2}{4}\left[\frac{v^n_{i+1/2,j} - 2v^n_{i+1/2,j-1/2} + v^n_{i+1/2,j-1}}{(\Delta y/2)^2}\right],$$

so that

$$|\tilde{u}^{n+1}_{i,j} - u^{n+1}_{i,j}| = O(\Delta t f \frac{\Delta x^2}{L^2} U).$$

This is the order of magnitude of the difference after one time step. The order of magnitude of the cumulative error after a characteristic time interval $T = f^{-1}$ is $O(U\Delta x^2/L^2)$.

5. CONCLUDING REMARKS

The equivalent formulation for the incompressible Navier-Stokes equations applied to the case in which the hydrostatic approximation is used, is attractive for numerical treatment. The described PGCM numerical method to solving the equivalent system has a number of advantages. The iteration method inside every time step, which is a generalized form of the predictor-corrector approach in SOMS, can be used for both Dirichlet and Neumann boundary conditions at the surface and bottom of the domain. It permits to evaluate the surface pressure and the vertical

diffusion implicitly, and assures that the velocity field is solenoidal at all times. Explicit treatment of the Coriolis term decouples the momentum equations in the implicit terms, and therefore avoids unwanted interpolations to different cells of the Arakawa-C grid, like in SOMS. This reduces the number of computational operations per time step, and above all avoids numerical diffusion.

The three-dimensional PROSPER general circulation model is characterized by: its exact conservation of mass in every time step; the speed of its algorithm, which permits a high resolution grid; and lack of numerical diffusion.

ACKNOWLEDGEMENTS

This research was initiated with a support of the Swiss National Science Foundation (grant nr.: 2.055.086) and continued within the framework of the PROSPER program (University of Neuchâtel, Switzerland) with the support of the Swiss Environmental Protection Office. It forms part of a thesis to be presented at the University of Neuchâtel. The author warmly thanks Dr. F.Nyffeler, Prof. O.Besson and Dr. R.Laydi for their contributions, and Dr. D.Dietrich, Dr. M.Marietta and Dr P.Roache for letting him use and study the Sandia Ocean Modelling System.

REFERENCES

1. D.E.Dietrich, M.G.Marietta and P.J.Roache,'An ocean modelling system with turbulent boundary layers and topography: numerical description',Int.J.Num.Meth.Fluids,7,833-855(1987).
2. K.Bryan,'A numerical method for the study of the circulation of the world ocean', J.Comp.Phys.,4,347-376(1969).
3. A.J.Semtner,'An oceanic general circulation model with bottom topography',NTIS PB 276 840.
4. E.A.H.Zuur and D.E.Dietrich,'The SOMS model and its application to Lake Neuchâtel', Aquatic Sciences, 52/2, 115-129(1990).
5. A.E.Gill,'Atmosphere-Ocean Dynamics',Academic Press (1982).

6. J.Pedlosky,'Geophysical fluid dynamics',Springer-Verlag,(1987)
7. P.M.Gresho and R.L.Sani,'On pressure boundary conditions for the incompressible Navier-Stokes equations',Int.J.Num.Meth. Fluids,Vol.7,1111-1145(1987).
8. S.Abdallah and J.Dreyer,'Dirichlet boundary conditions for the pressure poisson equation of incompressible flow', Int.J.Num. Meth.Fluids,Vol.8,1029-1036(1988).
9. O.Besson and R.Laydi, 'Some estimates for the hydrostatic approximation, and for the anisotropic Navier-Stokes equations', RAIRO,M^2AN (in press).
10. D.E.Dietrich, B.E.McDonald and A.Warn-Varnas,'Optimized Block-Implicit Relaxation',J.Comp.Phys.,18,421-439,(1975).
11. P.J.Roache,'Marching methods for elliptic problems', Num. Heat.Transfer,Vol.1,1-25(Part 1),163-181(Part 2) and 183-201 (Part 3)(1978).
12. P.J.Roache,'Computational fluid dynamics',Hermosa Publishers, (1982).
13. A.Arakawa and V.R.Lamb,'Computational design of the basic dynamical processes of the UCLA general circulation model', Meth.Comp.Physics,Vol.17,Academic Press,174-265(1977).

FIGURE CAPTION

Fig.1 Arakawa-C pressure control volume. $u_{i,j,k}$, $v_{i,j,k}$ and $w_{i,j,k}$ are drawn at the centers of the U-, V-, and W-control volumes, respectively. $u_{i,j,k+1/2}$ is drawn to illustrate the notation convention.

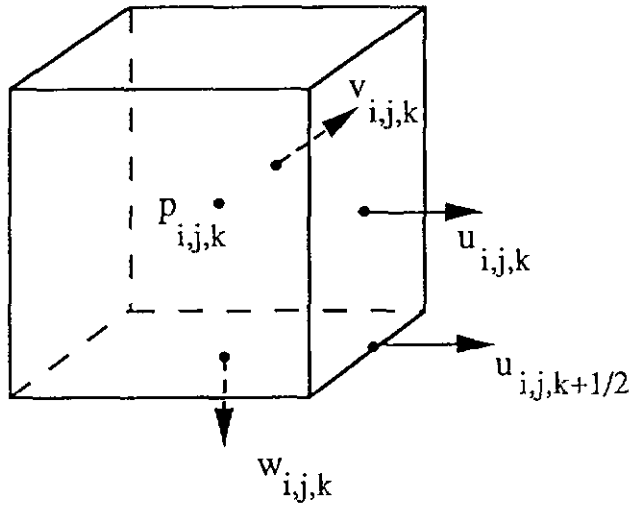

Fig. 1 Arakawa-C grid control volume for pressure

A NUMERICAL SIMULATION OF MESOSCALE DISPERSION IN THE DEEP OCEAN

E.A.H. Zuur[1], G.L. Weatherly[2], F. Nyffeler[1]

[1]*PROSPER, University of Neuchâtel (Switzerland)*
[2]*Dept. of Oceanography, Florida State University (U.S.A.)*

SUMMARY

Numerous benthic storms were observed during the Nord Ost Atlantisches Monitoring Programm (NOAMP), most of them being attributed to deep reaching mesoscale eddies. The Prosper General Circulation Model (PGCM) is used to simulate such an eddy. Realistic topography and thermal stratification are included in the model. The aim of this study is to investigate the combined effect of benthic storms and topography on the vertical transport in the deep ocean. In addition the dispersion of a dissolved tracer from a bottom source is simulated. It is shown that about half of the tracer is washed out of the well mixed benthic boundary layer locally and is dispersed vertically inside the eddy within 10 days.

1. INTRODUCTION

A benthic storm is loosely defined as a state in which the velocities near the bottom of the deep ocean are greater than 10 cm/s, and that lasts at least 48 hours. between September 1983 and may 1986 a monitoring program in the North-east-Atlantic was carried out under the name NOAMP (Nord-Ost-Atlatisches-Monitoring-

Programm). Its main purpose was to obtain field data in order to characterize deep ocean processes. During the experiment 20 benthic storms with velocities up to 27 cm/s and a duration between 3 and 25 days were observed in a region with horizontal area about 15000 km^2 and centered at 47°N20' and 20°W (Klein, 1987), here- after called the NOAMP-area. It was observed that most storms had a whirl-like structure and were obviously closely related to deep-reaching eddies. The average diameter of these eddies was found to be of the order of the local baroclinic Rossby deformation radius, being about 70 km. Besides the fact that benthic storms are energetic flows by definition, the measurements indicate that they are by no means exceptional, but exist a great deal of time.

In studying the dispersion of dissolved material from a source at the ocean-floor a number of stages can be identified (Robinson and Kupferman 1985). The first stage takes place in the benthic boundary layer. The BBL is the layer of water adjacent to the ocean bottom in which the vertical gradient of potential temperature is significantly smaller than in the deep-ocean interior. Its thickness varies between 30 and 100 m. Boundary-generated small- scale turbulence gives rise to intensive vertical and horizontal mixing of the fluid inside the BBL on time-scales small compared to those in the interior of the ocean (D'Asaro, 1982). In the second stage dispersive processes by mesoscale eddies begins, and material is sucked out of the BBL and transported into the ocean interior. In the third stage dispersal to basin and larger scales takes place by eddy diffusivity into isopycnal surfaces that outcrop at the sea surface at higher latitudes.

The aim of this study is to highlight the effect of a meso-scale eddy on the vertical upward dispersion of a passive tracer from the bottom into the interior of the deep ocean on a time-scale of days. So, in this paper attention is paid to the second stage of dispersion. As has been pointed out by Richards (1986) topography may strongly affect the flow-field induced by

meso-scale deep reaching eddies and should therefore be included in order to study these processes near the bottom. Instead of considering a field of eddies as was done by Richards (1986), we will only consider the flow-field and the resulting dispersion inside one eddy.

The problem is approached as follows. On account of velocity measurements performed during the NOAMP monitoring program a representative mesoscale eddy is simulated using the three-dimensional PROSPER General Circulation Model (PGCM) (Zuur, 1990). Realistic topography is included, as well as realistic thermal stratification according to hydrographical data from Mittelstaedt (1986). As a results of this, a dissolved tracer inside the BBL is dispersed into the interior of the ocean. It is assumed that at the start of the simulation the material is uniformly spread inside the BBL. The resulting distribution of material inside the eddy is discussed.

2. THE CIRCULATION MODEL

The PGCM is based on the Navier-Stokes equations, written in the primitive variables. Scaling estimates of the terms that appear in these equations justify the following approximations that simplify the resulting system (Gill, 1982; Pedlosky, 1987): The Bousinesq approximation; the hydrostatic approximation; the rigid lid approximation. Turbulence is represented by means of horizontal and vertical turbulent viscosity coefficients. ρ is the normalized density (i.e., density divided by reference density). The kinematic pressure (i.e., pressure divided by reference density) is denoted by a capital P. The resulting continuum equations are stated below.

- The horizontal momentum equations:

$$u_t + \nabla.(u\vec{v}) - fv = - P_x + A_H \nabla_h^2 u + A_V u_{zz},$$

$$v_t + \nabla.(v\vec{v}) + fu = - P_y + A_H\nabla_h^2 v + A_V v_{zz}.$$

- The hydrostatic approximation equation:

$$P_z = \rho g$$

- The mass conservation equation:

$$u_x + v_y + w_z = 0.$$

- The equation of state:

$$\rho = (1 - \beta(T - T_o)).$$

- The heat equation

$$T_t + \nabla.(T\vec{v}) = K_H\nabla_h^2 T + K_V T_{zz}.$$

The above equations apply to a bounded domain Ω for t>0, subjected to Dirichlet or Neumann boundary conditions at $\partial\Omega$ for the horizontal velocity components and temperature. Due to the hydrostatic approximation second order spatial derivatives of the vertical velocity component w have disappeared. A consistent boundary condition for w is $w.n_3 = 0$, in which n_3 is the third component of the outward unit pointing normal $\vec{n} = (n_1,n_2,n_3)$ at the boundary $\partial\Omega$. The initial conditions are:

$$\vec{v}(x,0) = \vec{v}_o(x) \quad \text{in } \bar{\Omega} \equiv \Omega \cup \partial\Omega,$$

with

$$\nabla.\vec{v}_o = 0 \quad \text{in} \quad \Omega,$$

and

$$T(\vec{x},0) = T_o(\vec{x}) \quad \text{in} \quad \bar{\Omega}.$$

A simple dispersion model is used to simulate the dispersion of a dissolved passive tracer from the BBL into the interior of the deep ocean. The transport equation for the this concentration

has the same form as the one for temperature:

$$C_t + \nabla.(C\vec{v}) = D_H\nabla_h^2 C + D_V C_{zz}.$$

The following symbols are used:

x, y, z	spatial coordinates in a left-handed Cartesian system (z-axes points downwards) [L];
t	time [T];
T	temperature [Θ];
u, v, w	velocity components ($\vec{v}$ = (u,v,w)) [LT^{-1}];
P	kinematic pressure [L^2T^{-2}];
ρ	normalized density;
g	effective gravitational acceleration [LT^{-2}];
A_H, A_V	turbulent viscosity coefficients [L^2T^{-1}];
K_H, K_V, D_H, D_V	eddy diffusion coefficients [L^2T^{-1}];
f	Coriolis parameter [T^{-1}];
β	coefficient of thermal expansion [Θ^{-1}];
∇	$\equiv (\partial/\partial x, \partial/\partial y, \partial/\partial z)$;
∇_h^2	$\equiv \partial^2/\partial x^2 + \partial^2/\partial y^2$.

The numerical integration method is based on an equivalent formulation of the above equations. Spatial integration is performed with a finite difference method and time integration is based on an extended form of the predictor-corrector method used in the Sandia Ocean Modeling System (Dietrich, Marietta, Roache, 1986). The three dimensional Eulerian grid is regular, but stretched in the vertical coordinate, in order to model accurately the effect of the bottom topography. The computational control volumes for different physical quantities, such as the pressure and the velocity components, are actually staggered in space, corresponding to the widely used Arakawa-C grid (Arakawa and Lamb 1977). For all relevant time dependent quantities the leapfrog

method is used. For an extensive description of the model we refer to Zuur (1990).

3. THE SIMULATION

Adjacent to the NOAMP area lies the Dumpsite area, which in the past has been used for the dumping of low-level radioactive waste. The Dumpsite's horizontal dimensions are 150 km along longitude and 115 km along latitude. The maximum depth of this open part of the North-east Atlantic Ocean is 4700 m. The Dumpsite is situated around 46^{o}N, 17^{o}W. The roughness of the bottom-topography is comparable with the NOAMP region and is characterized by mountains with maximum height of 1000 m, and a horizontal extension of 10 to 50 km (see fig.1 and fig.2).

The number of control volumes in a horizontal plane is taken NIxNJ=50x50. The lengths of the horizontal sides are Δx=3.10 km and Δy=2.28 km, respectively. The number of horizontal layers of control volumes is NK=20. The grid is stretched in the vertical coordinate: the thickness of the control volumes varies with depth from 1750 m for the top-layer to 81 m for the bottom layer (see table 1).

Table 1. Depth and thickness of stretched pressure control volumes:

K	z (m)	Δz (m)	K	z (m)	Δz (m)
1	1390	1750	11	3832	122
2	2003	455	12	3950	115
3	2375	319	13	4061	108
4	2657	254	14	4167	103
5	2889	214	15	4267	98
6	3089	187	16	4363	94
7	3266	168	17	4455	90
8	3425	152	18	4543	86
9	3571	140	19	4628	83
10	3706	130	20	4710	81

With the horizontal resolution, the smallest scale horizontal eddies resolved by the grid are significantly non-hydrostatic. However, the flows generated in this study are generally dominated by much larger scale horizontal variations and therefore are quasi-hydrostatic. Thus, the hydrostatic model used here is a reasonable approach. Later, Non-hydrostatic effects could be included in the model in a way as described by Dietrich, Marietta and Roache (1987).

The grid near the bottom is too coarse to resolve the bottom boundary layer. The Ekman layer thickness $\pi\sqrt{(2A_V/f)} \simeq 12$ m is much smaller than the lowest grid-layer. Setting a no-slip condition at the bottom is not appropriate then. Therefore, a drag law is used. The bottom shear stress is related to the velocity in the bottom layer according to

$$(\tau_{bx},\tau_{by}) = \rho_o C_D^2 \sqrt{(u_b^2 + v_b^2)}\ (u_b,v_b),$$

in which (u_b,v_b) is the horizontal velocity in the last layer. The drag-coefficient is taken C_D=0.035. The resulting boundary condition at the bottom is

$$\rho_o A_V (\frac{\partial u}{\partial z},\frac{\partial v}{\partial z}) = (\tau_{bx},\tau_{by}).$$

Orlanski's free radiation boundary condition is used at the open sides of the domain (Orlanski, 1976). This condition avoids reflection of topographic waves from the open boundary sides.

Heat fluxes are kept zero at the boundary of the domain. The initial vertical temperature gradient is taken constant: $\partial T/\partial z$=0.1 ^{o}C/km.

A cyclonic eddy is generated numerically inside the Dumpsite by applying wind stress at the surface of the domain. Of course, in reality the main cause of mesoscale eddies involves fluid

instability rather then direct wind stress driving. However, for the purposes of determining characteristic mixing time scales near the bottom, a reasonable first step for a limited open high resolution calculation is to artificially drive such eddies by wind stress.

It is noted that the Ekman layer at the surface is not resolved by the model and that the initial vertical temperature gradient is realistic only for the lower part of the ocean. Therefore, the energy-transfer in the model from the surface to the bottom will not be realistic in the upper layer. However, our interest is not in the processes in this layer, but in the mesoscale dispersion in the lower part of the Dumpsite domain. So, the wind-forcing at the surface is only a means to generate an eddy in the deep ocean in which the horizontal length scale and velocities are comparable with those observed by Mittelstaedt et al. (1986) and Klein (1987) during a benthic storm.

First the model is spun up during 10 days in order to generate the eddy. Then, during the next 10 days, dissolved material, initially uniformly distributed over the 81 m thick benthic boundary layer in the valley of the Dumpsite (being the black part in fig.1), is dispersed into the interior of the Dumpsite region due to the eddy-activity. Fluxes of this material are kept zero at the top and bottom of the domain, and normal gradients are kept zero at the open sides.

Parameters used in the calculations have the following values:

- Reference density : ρ_o = 1 gr/cm^3;
- Horizontal turbulent viscosity : A_H = 5x10^6 cm^2/s;
- Vertical turbulent viscosity : A_V = 10 cm^2/s;
- Horizontal eddy diffusion for heat : K_H = 10^6 cm^2/s;
- Vertical eddy diffusion for heat : K_V = 1 cm^2/s;
- Horizontal eddy diffusion for concentr. : D_H = 5x10^6 cm^2/s;
- Vertical eddy diffusion for concentr. : D_V = 10 cm^2/s;

- Coriolis parameter : $f = 10^{-4}\ s^{-1}$;
- Gravitational acceleration : $g = 980\ cm/s^2$;
- Coeff. of thermal expansion : $\alpha = 2 \times 10^{-4}\ {}^{o}C^{-1}$;
- Time step : $\Delta t = 450$ s.

The conditions for the PGCM model to be stable are given in Zuur (1990). With the above time-step the stability of the calculations is quaranteed. Small variations of the vertical turbulent viscosity coefficient have little influence on the results, since the vertical transport is primarily advective. Variations of the horizontal turbulent viscosity coefficient have a stronger influence on the resulting velocity field. Although the velocity field is smoothed by increasing this coefficient, it has little influence on the total quantity of matter that is dispersed over the considered period of time.

4. RESULTS

The results that are presented, describe the situation after 10 days of material dispersion due to eddy-activity.

Fig.3 shows the eddy-field at three depth-levels: 387 m, 207 m and 40 m above the bottom, respectively. The center of the eddy at these depths does not longer coincide with the center of the horizontal planes as it does near the surface, but has shifted towards the north-west above the valley. The maximum velocity above the benthic boundary layer is about 10 cm/s.

Initially the tracer is uniformly spread over the 81 m thick last depth-layer (i.e., for k=20) in the valley of the Dumpsite with concentration C = 100. During 10 days the material is dispersed inside the eddy. The resulting dispersion extends to about 500 m above the bottom. The concentration is shown in fig.4 at three depth- levels. The mean concentration at a level is denoted CMEAN, and the maximum concentration CMAX. The mean concentration inside the last depth-layer at 4710 m (40 above the

bottom) is CMEAN=52.67, so that about half of the tracer has been washed out of this layer over a period of 10 days.

5. CONCLUDING REMARKS

Benthic storms observed during the NOAMP monitoring program, indicate high activity of deep reaching eddies in the North-east Atlantic. The performed numerical simulation illustrates the combined effect of such an eddy and topography on the dispersion of dissolved material from the well mixed BBL into the interior of the eddy. About half of the material is washed out of the BBL and dispersed inside the eddy over a 500 m thick layer above the bottom within 10 days. The simulation shows the effectiveness of the considered process in transporting material to higher levels in the deep ocean.

Since the simulated type of circulation process is not exceptional in the North-east Atlantic, its effect on the vertical transport of material should be taken into account when studying dispersion on a larger (ocean-wide) scale.

ACKNOWLEDGEMENTS

This research was initiated with a support of the Swiss National Science Foundation (grant nr.: 2.055.0B6) and continued within the framework of the PROSPER program (University of Neuchâtel, Switzerland) with the support of the Swiss Environmental Protection Office. The authors warmly thank Dr. D.E.Dietrich and Dr. E.Mittelstaedt for their valuable comments.

REFERENCES

Arakawa, A. and V.R.Lamb, 1977. 'Computational design of the basic dynamical processes of the UCLA general circulation model', Methods in Computational Physics, Vol.17, Academic Press, pp. 174-265

D'Asaro, E., 1982. Velocity structure of the benthic ocean. J. Phys. Oceanog., 12, 323-336.

Dietrich, D.E., M.G.Marietta and P.J.Roache, 1987. 'An Ocean Modeling System with Turbulent Boundary Layers and Topography', International Journal for Numerical Methods in Fluids, vol.7, 833-855.

Gill, A.E., 1982. 'Atmosphere-Ocean Dynamics', Academic Press.

Klein, H., 1987. 'Bentic Storms, Vortices and Particle Dispersion in the deep West Europian Basin', Dt.hydrogr.z.40.

Mittelstaedt, E. (ed.), M.Bock, I.Bork, H.Klein, H.Nies, U.Schauer, 1986. 'Ausbreitungbedingungen für Stoffe in grossen Tiefen (NOAMP- Nordostatlantisches Monitoring-Programm)', Hamburg: Deutches Hydrogr. Institut. 202 S. m. Abb. u. Tab.

Pedlosky, J.,1987. 'Geophysical Fluid Dynamics', Spriger Verlag New York.

Orlanski, I., 1976. 'A simple boundary condition for unbounded hyperbolic flows', J. Comp. Physics, 21, pp 251-269.

Richards, K.J., 1986. 'Dispersion of tracers by the oceanic eddy field'. Inst. of Ocean. Sciences, Wormley, I.O.S. report No. 229

Robinson, A.R. and S.L. Kupferman, 1985. 'Dispersal from deep ocean sources: Physical related processes', Sandia-report, SAND82-1986.

Zuur, E.A.H., 1990. 'The Prosper General Circulation Model, a Numerical Description'. Int.J.Num.Meth.Fluids (in press).

FIGURE CAPTIONS

Fig.1. Dumpsite topography.

Fig.2. Contour plot of Dumpsite topography. The distance between tickmarks represent the length of the sides of the gridcells.

Fig.3. Horizontal velocity field at three depth-levels.

Fig.4. Concentration field at three depth-levels.

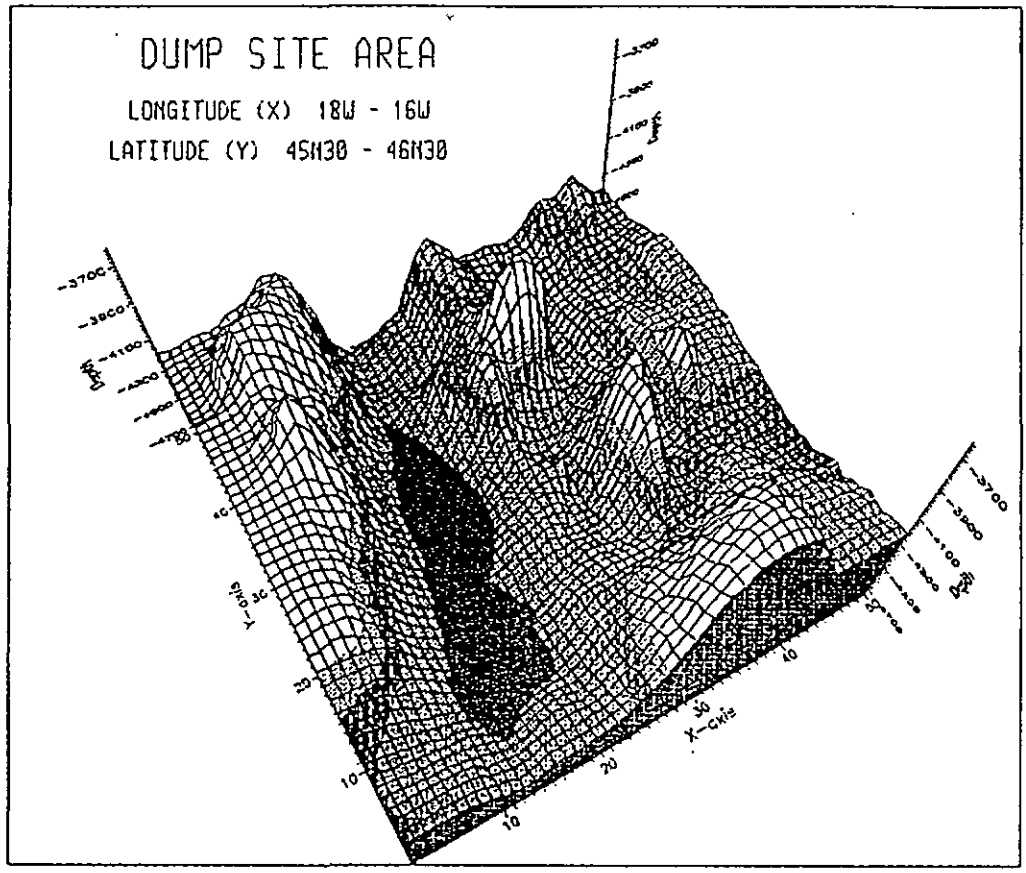
DUMP SITE AREA
LONGITUDE (X) 18W - 16W
LATITUDE (Y) 45N30 - 46N30

Fig.1.

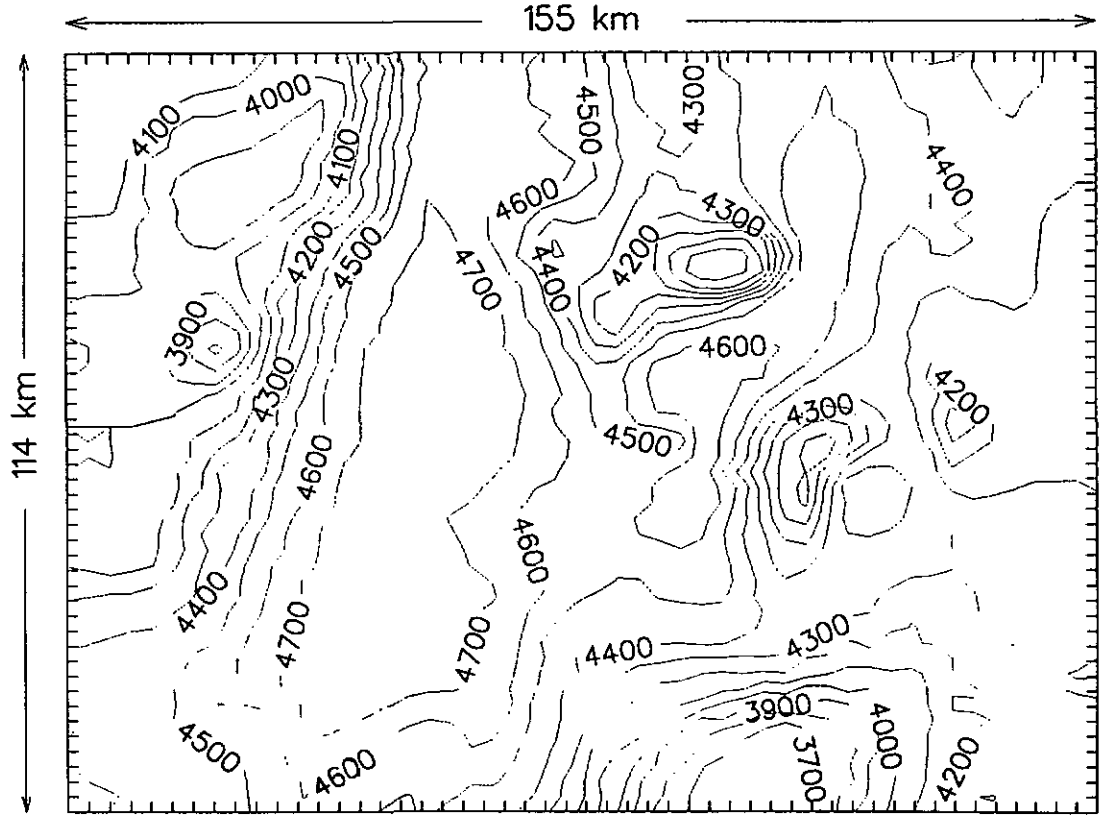
155 km
114 km
4100
4000
4100
4200
4500
3900
4300
4600
4700
4500
4600
4400
4200
4300
4400
4600
4500
4300
4200
4600
4400
4700
4600
4700
4400
4300
3900
4000
3700
4200
4500
4600

Fig.2.

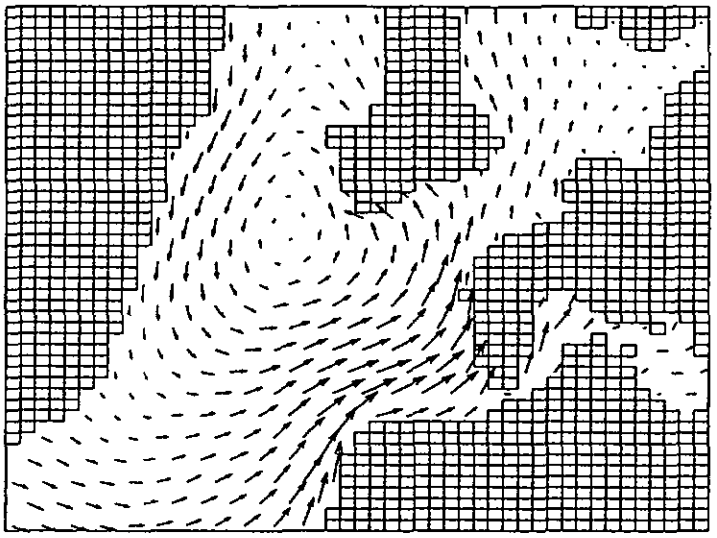

K= 16 Depth (m)= 4363 VMAX (cm/s)= 10.34

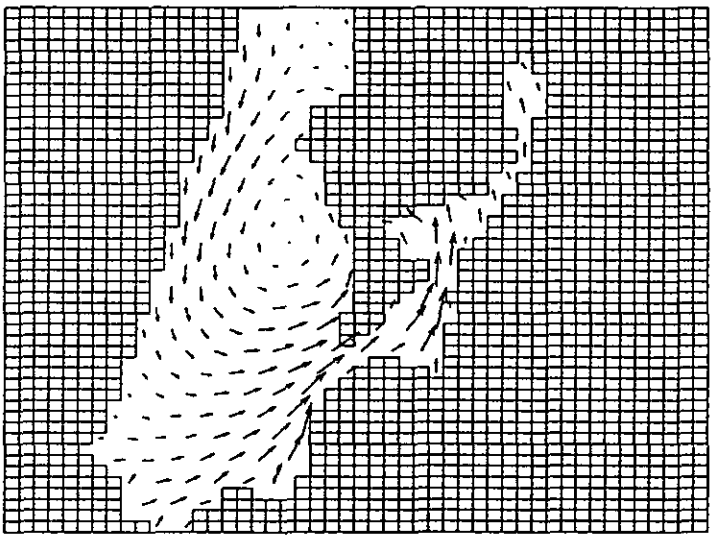

K= 18 Depth (m)= 4543 VMAX (cm/s)= 10.94

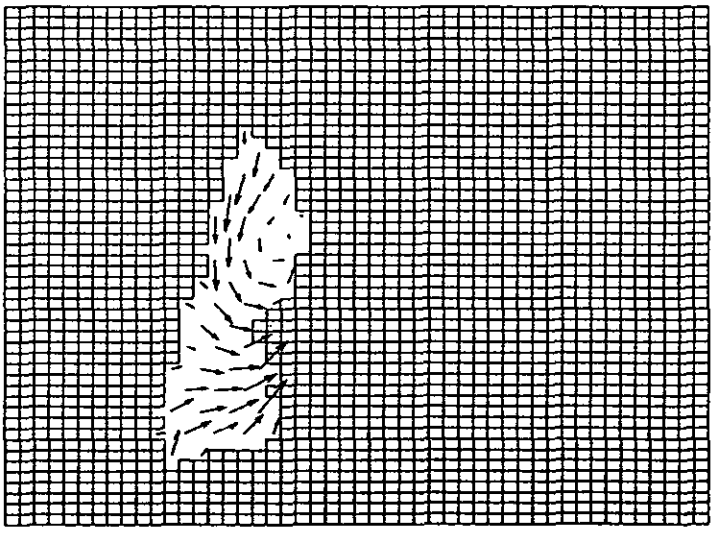

K= 20 Depth (m)= 4710 VMAX (cm/s)= 5.80

Fig.3.

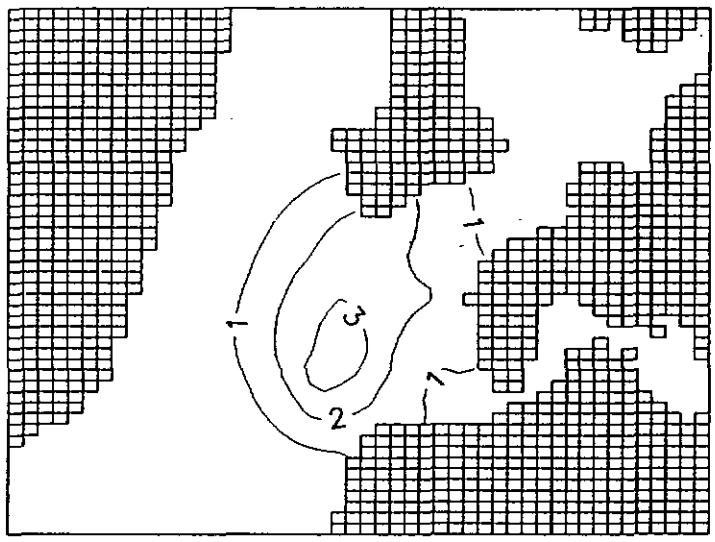

K= 16 Depth (m)= 4363 CMEAN= 0.62 CMAX= 3.53

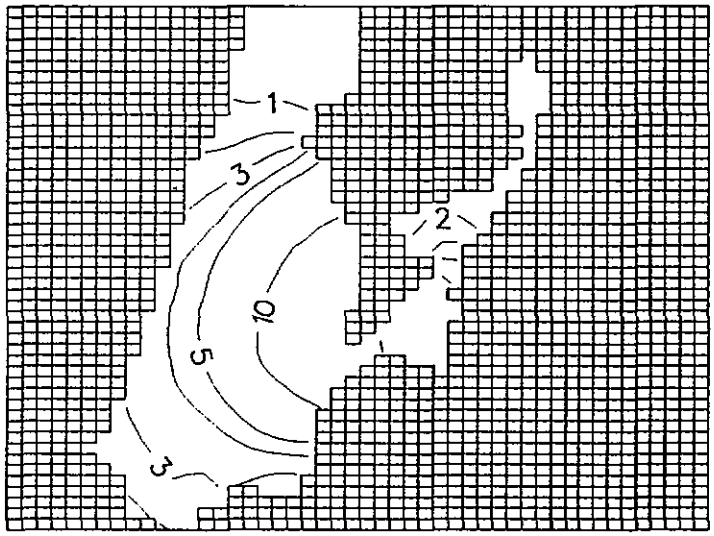

K= 18 Depth (m)= 4543 CMEAN= 4.75 CMAX= 14.90

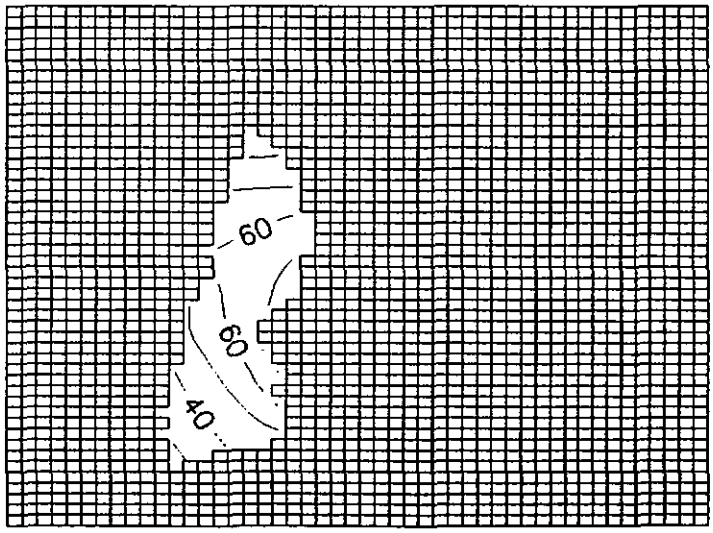

K= 20 Depth (m)= 4710 CMEAN= 52.67 CMAX= 71.90

Fig.4

THEORETICAL SUSPENDED PARTICLE DISTRIBUTIONS IN OPEN OCEAN SYSTEMS; A COMPARISON WITH OBSERVATIONS

E.A.H. Zuur, F. Nyffeler
PROSPER, University of Neuchâtel (Switzerland)

ABSTRACT

The vertical distribution of suspended particulate matter measured by filtration/weighing or by continuous optical profiling exhibits similar trends in large areas of the open ocean. A mathematical model is presented to determine the number of particles per unit volume and the particle size-distribution as functions of depth, when this number and this distribution are prescribed at the surface and/or at the bottom. The influence of dissolution, adsorption, splitting and aggregation of particles is assessed, and theoretical nephelometric profiles are derived. Comparison with data from the open North-East Atlantic demonstrates that the effect of dissolution alone, in connection with the dynamical behaviour of the particles, is sufficient to obtain the general trend of the experimental profiles.

1. INTRODUCTION

Since about three decades, there is an increasing interest for suspended particulate matter (SPM) in the ocean in the fields of biology, chemistry, geochemistry and physics. One of the challenges of the early years was the description of the general distribution of the SPM in the oceans. Because sampling and filtration are time consuming tasks, varies types of optical

devices (attenuance-, scattering- and turbidity-meters) have been developed to provide reliable estimates of the quantity of SPM in the sea-water. The first comprehensive map of turbidity in the Atlantic Ocean was presented by Ettreim *et al.* (1976), on the basis of more than a thousand light scattering profiles acccumulated since 1967 by the Lamont Doherty Geological Observatory. In a second paper Biscaye and Ettreim (1977) converted these data in terms of weight of the SPM, and gave estimates of the suspended loads and transports in the bottom nepheloid layer. From these observations a general trend was identified, described as a strong decrease of the turbidity with depth directly below the biologically active surface layer, a further decrease with an almost constant weak gradient down to the 'clear water minimum', and then an increase of the turbidity towards the bottom.

A variety of chemical, biological and dynamical processes that relate to particulate matter are carefully described and reviewed in a paper by Lal (1977). This paper not only summarizes the state of the art, but also provides various particle-related parameters, updated on the basis of the extensive experimental work carried out during the GEOSECS program. These data will be used as input to the mathematical model that will be derived in this paper. More recently, the role of each of the processes contributing to the change in the particle size-distribution in the ocean was individually examined and discussed by McCave (1984) on the basis of a comprehensive bibliography of over a hundred references. Here, we will not consider the chemical and biological processes in detail, but we will assume that their resultant integral effect on the particulate matter can be described in a relatively simple but sensible way.

Let us outline the basic concepts used in this paper. Apart from pure water, the ocean also contains mass of another origin, such as salt and organic matter. This mass either exists in the form of particles or is dissolved in the fluid. From a dynamical point of view, the difference in form is characterized by the

different resultant forces that act on the mass. For a particle, these forces are the gravity and a frictional force on its surface exerted by the surrounding fluid. In case the mass is dissolved, the forces exerted by the fluid have a direct electro-magnetic nature. Since at a short range the electro-magnetic forces are strong, the dynamics of the dissolved mass and of the fluid are indistinguisable, while the dynamics of a particle may well differ from that of the surrounding fluid.

We will look at four major categories of processes with respect to the changes in size of particles. The first category comprises those processes by which the mass of a particle is gradually dissolved into the fluid and by which, as a consequence, its size dimineshes in time. The counter-part of dissolution is the fixation of dissolved matter onto a particle, which results in an increase of its size. Let us call it adsorption. The third category covers processes leading to a splitting of particles into smaller parts, and the fourth to the aggregation of particles. The four categories are represented schematically in fig.1.

In the first two groups the number of particles remains the same (as long as the particles are not completly dissolved), while the mass of the particulate matter undergoes a change. In the last two processes, the mass of the particulate matter remains unaffected, while the number of particles changes. This determines the type of conservation principle that will be applied when these different categories are considered: conservation of the number of particles for dissolution and adsorption, and conservation of the mass of the particulate matter for splitting and aggregation.

In a simple fluid (such as water), molecules loose their identity if the properties of the fluid are looked at on a macroscopic scale. At this scale, the fluid is treated as a continuum and individual molecules do no longer play an explicit role. The same in general is true if one studies the evolution of the concentration (i.e., the mass per unit volume) of dissolved matter. In studying the behaviour of particles, however, one

cannot be concerned with their concentration alone, but one should take into account the size-distribution of the particles that contribute to this concentration. This will give rise to some additional problems in deriving the equations that determine the state of particle population as a function of time and location in the water column, when appropriate initial and boundary conditions are prescribed.

2. BASIC EQUATIONS

2.1 Hypotheses

Consider a column of fluid V. Assume that the magnitude of any relevant physical quantity in V only depends on the vertical depth coordinate z (z-axis is pointing down-wards). This comes down to saying that we deal with a horizontally homogeneous open ocean system. Particles in the fluid are supposed to be spherical. They are acted on by gravity and a frictional force exerted at the surface by the surrounding fluid. We will not take into account the acceleration of a particle due to these forces, but assume the state in which the resultant force is zero. This will be the case if the particle has a certain velocity w. We suppose that the only variable quantity on which w depends is the particle's radius, so we have $w=w(R)$. Note that in this way w may also depend on a constant vertical velocity of the fluid. Further, w is taken to be a strictly increasing continuous function for all $R\in(0,\infty)$.

The basic equations are established for the case where all particles in V dissolve. The derivation is similar for the other categories of processes, although some subtle differences will be pointed out in section 2.4.

2.2 Input of particles at the surface with the same radii

Apart from its movement, a particle gradually dissolves in the fluid. The size-rate D is defined as the change in radius per unit

time. It is assumed that it only depends on the radius itself, so we have $D(R)=dR/dt$, and that $D(R)$ is a continuous function for all $R\in(0,\infty)$. From the definition of dissolution it follows that $D(R)$ must be a negative function for all $R\in(0,\infty)$.

Let there be a permanent input of particles at the surface of V, at $z=0$, all particles having the same radius R_o at the moment they enter the volume. Depth z as a function of R is given by

$$z(R) = \int_0^t w(R(t))dt = \int_{R_o}^{R} w(R)\frac{dt}{dR}(R)dR = -\int_{R}^{R_o}\frac{w(R)}{D(R)}dR. \qquad (1)$$

Since w is a strictly increasing function, the equation $w(R)=0$ may have one solution, say for $R=\varkappa$. Then, $w(R)$ is negative for all $R\in(0,\varkappa)$, and positive for all $R\in(\varkappa,\infty)$. Particles must have a positive velocity to enter V at the surface, and therefore we must have $R_o>\varkappa$. The maximum depth that a particle reaches, is at the moment $w(R)=0$, i.e., for $z=z(\varkappa)$, and the depth at which a particle dissolves completly is at $z=z(0)$. Now, let it be given that $R\in(\varkappa,R_o)$. Since $D(R)$ is negative for all R, the integrand $w(R)/D(R)$ is one-signed in this interval. Then, (1) determines R uniquely as a function of z, for all $z\in(0,z(\varkappa))$. On the other hand, let $R\in(0,\varkappa)$. We rewrite (1) in the form

$$\int_R^{\varkappa}\frac{w(R)}{D(R)}dR = -\int_{\varkappa}^{R_o}\frac{w(R)}{D(R)}dR - z(R) = z(\varkappa) - z(R).$$

The right hand side is positive, since $z(\varkappa)$ is the maximum depth. The integrand at the left hand side is positive for all $R\in(0,\varkappa)$. So, in this case there is also one and only one R for any given $z\in(z(0),z(\varkappa))$. In other words, given that R belongs to one of the intervals $(0,\varkappa)$ or $(\varkappa,R_o)$, the relation between R and z is bijective.

Let A be a control volume in V, bounded by an upper surface z and a lower surface $z+\Delta z$. Further, consider the time-interval between t and $t+\Delta t$. Let $N(R,t)$ denote the number of particles per

unit volume with radius R at time t. N is assumed to be continuous for all $R\in(0,\infty)$ and for all $R\in(\infty,R_o)$. The derivation below of the continuity equation for N applies to each of the seperate intervals. In case $R\in(\infty,R_o)$, control volume A is assumed to be in the depth interval $(0,z(\infty))$, while if $R\in(0,\infty)$, A is assumed to be in the interval $(z(0),z(\infty))$.

Given that R is either in $(0,\infty)$ or in (∞,R_o), R may be considered to be a function of z, i.e., R=R(z). On account of the mean-value theorem of integral calculus, the flux of particles through a unit surface at depth z during Δt is

$$w(R(z))N(R(z),\bar{t})\Delta t,$$

for some $\bar{t}\in(t,t+\Delta t)$, and the flux at depth $z+\Delta z$ is

$$w(R(z+\Delta z))N(R(z+\Delta z),\bar{t})\Delta t.$$

Although in general the $\bar{t}$'s in the expressions above have different values, both are elements of $(t,t+\Delta t)$. For a matter of convenience we will make no distinction in notation. Since there is no production of particles in A, the increase of the number of particles during Δt is

$$\Delta N(R(\bar{z}),\bar{t})\Delta z = w(R(z))N(R(z),\bar{t})\Delta t - w(R(z+\Delta z))N(R(z+\Delta z),\bar{t})\Delta t,$$

with $\bar{z}\in(z,z+\Delta z)$. This holds for an arbitrary control volume A and an arbitrary time-interval. By dividing by Δz and Δt and by taking $\Delta z\to 0$ and $\Delta t\to 0$ we obtain the continuity equation for the number of particles per unit volume, in case all particles at the surface have the same radius:

$$\frac{\partial N}{\partial t} + \frac{\partial wN}{\partial z} = 0.$$

If N is prescribed at the surface of V and independent of t (say $N=N_o$ for $R=R_o$), the continuity equation permits stationary

solutions in both $(0,\varkappa)$ and $(\varkappa,R_o)$. The residence-time of particles in the water-column, in particular of small ones, is so long compared to the seasonal fluctuations of particle production near the surface, that the stationary state approximation is justified in the open ocean. Therefore, in the remainder we will only consider the stationary state, and we set

$$\frac{\partial N}{\partial t} = 0.$$

With (1), dz is expressed in terms of dR:

$$dz = \frac{w(R)}{D(R)}dR,$$

and we get

$$\frac{dwN}{dR} = 0.$$

The boundary condition at the surface, being the condition with respect to the interval $(\varkappa,R_o)$ at $R=R_o$, is prescribed above. The remaining boundary condition with respect to the interval $(0,\varkappa)$ is the continuity of the magnitude of the flux of particles $|w|N$ at $R=\varkappa$. We find

$$|w(R)|N(R) = w(R_o)N_o \quad \text{for} \quad 0 < R \leq R_o.$$

For the number of particles per unit volume in the stationary state we finally get

$$N(R) = N_o \frac{w(R_o)}{|w(R)|} \quad \text{for} \quad 0 < R \leq R_o \text{ and } R \neq \varkappa, \qquad (2)$$

2.3. Input of particles at the surface with different radii

Instead of considering all particles to have radius R_o at the surface, let's consider the case in which there are N_o particles per unit volume at the surface with different radii. Let $P(R_o)$ be a particle size-distribution, such that $P(R_o)>0$ for $R_o>0$ and

$$\int_0^\infty P(R_o)dR_o = 1.$$

In order to obtain the number of particles per unit volume as a function of z, and to derive the size-distribution at this depth, dR_o will be expressed in terms of dR for fixed z. With (1), the depth-location of a particle with radius R that originaly had radius R_o at the surface is

$$z(R;R_o) = \int_{R_o}^{R} \frac{w(R)}{D(R)}dR.$$

And so

$$dz(R;R_o) = \frac{w(R)}{D(R)}dR - \frac{w(R_o)}{D(R_o)}dR_o.$$

For fixed z we have dz=0, thus

$$dR_o = \frac{w(R)}{w(R_o)}\frac{D(R_o)}{D(R)}dR = \frac{|w(R)|}{w(R_o)}\frac{D(R_o)}{D(R)}|dR|. \qquad (3)$$

The last equality is due to the fact that dR_o is considered to be positive. As already mentioned, for particles at the surface to enter V we must have $R_o>\varkappa$. Rewrite (1) in the following form:

$$\int_{\varkappa}^{R_o} -\frac{w(R)}{D(R)}dR = \int_{R}^{\varkappa} \frac{w(R)}{D(R)}dR + z. \qquad (4)$$

It is readily verified, that the right hand side is positive for R>0 and z>0. Further, the integrand at the left hand side is positive for $R>\varkappa$. So, there is one and only one $R_o>\varkappa$ that satifies the above equation for given R and z, and we may write $R_o=R_o(R,z)$.

Let N(z) denote the number of particles per unit volume at

depth z. With (2), the increase of N(z) due to particles that initially had radii between $R_o(R,z)$ and $R_o(R,z)+dR_o$ at the surface is

$$dN(z) = N_o \frac{w(R_o(R,z))}{|w(R)|} P(R_o(R,z))dR_o.$$

By expressing dR_o in terms of dR for fixed z with (3), and by integrating over all R, we obtain

$$N(z) = N_o \int_0^\infty \frac{D(R_o(R,z))}{D(R)} P(R_o(R,z))dR. \qquad (5)$$

The particle size-distribution at depth z follows immediately from the above expression, and is given by

$$P(R;z) = \frac{N_o}{N(z)} \frac{D(R_o(R,z))}{D(R)} P(R_o(R,z)). \qquad (6)$$

Since N(z) and P(R;z) determine the state of the particle population completly, any quantity or distribution related to this population can be derived from them.

2.4 Absorption, splitting and aggregation

The number of particles per unit volume and the size-distribution are derived along the same lines for adsorption, splitting and aggregation. In case that particles adsorb dissolved matter, the size-rate D(R) is a positive, instead of a negative function as for dissolution. In case of splitting (D(R)<0) or aggregation (D(R)>0) of particles, the derivation is based on the principle of conservation of mass. For a continous splitting process, however, the number of particles per unit volume will tend to infinity.

To see this, consider the splitting process. If all particles

have the same radius R_o at the surface, for the mass-flux we find in an analog way as in section 2.2 that

$$|w(R)|M_p(R) = w(R_o)M_p(R_o) \quad \text{for} \quad 0 < R \leq R_o,$$

in which $M_p(R)$ is the mass of the particles with radius R per unit volume, and $M_p(R_o)$ the prescribed mass-density of particles with radius R_o. Now, let m(R) be the mass of a particle with radius R, then $M_p(R)=m(R)N(R)$. For the number of particles per unit volume we then find

$$N(R) = N_o \frac{m(R_o)}{m(R)} \frac{w(R_o)}{|w(R)|} \quad \text{for} \quad 0 < R \leq R_o \text{ and } R \neq \varkappa.$$

If a size-distribution is prescribed at the surface, we find for the number of particles at depth z with radii greater than a>0

$$N(z) = N_o \int_a^\infty \frac{D(R_o(R,z))}{D(R)} \frac{m(R_o)}{m(R)} P(R_o(R,z))dR. \qquad (7)$$

A minimum radius R=a must be introduced in the case of a continuous splitting process, because if R tends to zero, m(R) tends to zero and N(z) will tend to infinity. For the corresponding size-distribution we get

$$P(R;z) = \frac{N_o}{N(z)} \frac{D(R_o(R,z))}{D(R)} \frac{m(R_o)}{m(R)} P(R_o(R,z)) \quad \text{for } R > a.$$

2.5 Short comments on the four categories of processes

In order to keep the approach tractable we only considered the resultants of well defined types of processes. One important question is thus: does one of the four categories dominates the others in the ocean below the productive surface layer and above

the near-bottom layer?

In the clear oceanic water, the SPM concentration ranges between 10 to 20 $\mu g/dm^3$. As a consequence, the average distance between individual particles is large compared to their radii, and aggregation is not believed to be a mostly efficient process. By assimilating nutrients from the seawater, microorganims put dissolved mass into particulate form, a process which is included in our definition of adsorption. This type of process mainly occurs in the upper biogenic layer, but is of limited influence in the underlying water. Splitting of particles will also definetely be important in the upper layer of the ocean, for example through the desintegration of fecal pellets. But as was noticed in section 2.4, if particles get smaller and smaller by a continous splitting process, their number per unit volume tends to infinity. This is not in agreement with observations in the submicron range (Lambert *et. al*, 1981). The introduction of an artificial minimum radius $a>0$ in (7) comes down to saying that particles with radii smaller than a are dissolved. So, a splitting process must end up in a dissolution process.

On account of these generic considerations, in the remainder of this paper, we will assume dissolution to be the dominant category of processes. We will apply the model by making use of parameter estimates provided by Lal (1977).

3. SPECIFICATION OF FUNCTIONS AND PARAMETERS

3.1. The size-rate and settling velocity

It is a well known fact, that different sorts of particles dissolve with different rates, and in particular that lots of particles hardly dissolve at all (Lal 1977). In the stationary state, this later group forms a uniform 'curtain' of particles in the water column. That is, since they hardly dissolve, their size and number per unit volume is independent of depth. We will

consider one class of particles, all having the same constant dissolution-rate. Although, this may not reflect reality in a very accurate way, it makes the results more accessible to interpretation.

The simplest and most common model to describe dissolution of particles is one with a constant dissolution-rate (Lal 1977). The radius as a function of time is given by

$$R(t) = \begin{cases} R_o - \varepsilon t & \text{for} \quad t \leq R_o/\varepsilon, \\ 0 & \text{for} \quad t > R_o/\varepsilon. \end{cases}$$

The resulting size-rate is

$$D(R) = \frac{dR}{dt}(R) = -\varepsilon \quad \text{for} \quad 0 < R \leq R_o.$$

Stokes' law for the resistance of a moving sphere (Batchelor 1967) is often applied with respect to the settling velocity of particles (Lerman *et al.* 1974, Brun-Cottan, 1976). Further, the fluid may have a constant upward velocity u, the magnitude of which was suggested by Munk (1966) for the Central Pacific. So, for the velocity of a particle with radius R we get

$$w(R) = \beta R^2 - u,$$

with

$$\beta = \frac{2}{9} \frac{g}{\nu} \left(\frac{\rho}{\rho_f} - 1\right).$$

g is the gravitational acceleration, ν the kinematic viscosity of the fluid, ρ the mass-density of the particle, ρ_f the mass-density of the fluid, and u the background velocity (taken positive upwards). If u is positive, one sees that w changes sign if $R=\varkappa=\sqrt{(u/\beta)}$.

Instead of determining $R_o(R,z)$ numerically with (4), in case of the above definitions of D(R) and w(R), this function can also

be found analytically from a third degree polynomial. With (1), we have

$$z = \int_{R_o}^{R} \frac{w(R)}{D(R)} dR = -\frac{1}{\varepsilon} \left[\frac{\beta}{3}(R^3 - R_o^3) - u(R - R_o)\right],$$

and by rearranging terms we get

$$R_o^3 - \frac{3u}{\beta} R_o = R^3 - \frac{3u}{\beta} R + \frac{3\varepsilon}{\beta} z.$$

There exists exactly one root $R_o > \varkappa = \sqrt{(u/\beta)}$ for all $R>0$ and $z>0$.

The following values correspond to the values given by Lal (1977):

- dissolution rate : ε = 0.15 μm/y;
- Munk's value for background velocity : u = 0.14 μm/s;
- gravitational acceleration : g = 9.81 m/s^2;
- kinematic viscosity : ν = 0.015 cm^2/s;
- density particle : ρ = 1.5 g/cm^3;
- density water : ρ_f = 1.0 g/cm^3;

3.2 The particle size-distribution

In the biologically active surface layer many different kind of processes play a role that depend on seasonal fluctuations. The resultant effect of these processes is, however, to establish a more or less stationary particle size-distribution in the lower part of this layer at about 100 meters below the ocean surface. The particle size-distribution that has to be specified at the surface of the water-column V (section 2.3) should therefore correspond to the one observed in the ocean at that depth.

The particle size-distribution in the lower part of the productive layer of the ocean is usually described by a power law

(Bader 1970, Brun-Cottan 1976, McCave 1983). As far as we know, this choice is not based on theoretical considerations, but merely corresponds to a convenient way to fit experimental data in the size range covered by particles counters (e.g., the Coulter Counter). Since a power law distribution is either cutoff before zero, or tends to infinity if R_o tends to zero, it is unlikely that it remains valid for small radii. Therefore, as a basic distribution we will take the exponential distribution. This distribution is bounded for $R_o=0$, and the difference with a power law distribution in any interval (α,∞), with $\alpha>0$, can in general be made extremely small by adjusting its mean. The exponential distribution has the form

$$f_\theta(R) = \frac{1}{\theta} e^{-R/\theta} \qquad \text{for} \quad R \geq 0,$$

in which θ is the mean radius.

Measurements of particle repartitions obtained with the Coulter Counter are usually displayed as volume density distributions, with the radius axis represented on a logaritmic scale. In such graphs two peaks are often depicted below the productive surface layer, which corresponds to a bimodal distribution. This implies, that the particle size-distribution is also bimodal, and we set

$$P(R_o) = (1-\omega) f_{\theta_1}(R_o) + \omega f_{\theta_2}(R_o), \qquad (8)$$

where ω is the weight coefficient between the two modes, with $\omega\in[0,1]$.

The mean of the first mode is determined by a best fit of this mode with the usual power law distribution. We obtain $\theta_1=0.4$ μm. Since the second mode is in practice only visible through the volume density distribution, we will fit the theoretical volume density distribution with observations in order

to determine θ_z and ω.

The theoretical cumulative volume density distribution of the particles is defined as:

$$V_p(R;z) = N(z)\frac{4}{3}\pi\int_0^R R^3 P(R;z)dR;$$

the volume density is

$$V_p(z) = \lim_{R\to\infty} V_p(R;z);$$

and the corresponding volume density distribution is

$$\frac{1}{V_p(z)}\frac{\partial V_p(R;z)}{\partial R} = \frac{N(z)}{V_p(z)}\frac{4}{3}\pi R^3 P(R;z). \qquad (9)$$

A series of volume density distributions measured in the N.E. Atlantic ($40^oN/20^oW$) by Nyffeler and Ruch (1989) have been used to estimate the mean of the second mode and the weight coefficient. Good fits were obtained with θ_z=2 μm and ω=0.0025.

3.3 The total light-scattering coefficient

The scattering of light by particles is used as an indication for the particle content. The scattered intensity depends on the number per unit volume, on the size of the particles, and to a minor extend on their shape and index of refraction. For a population of spherical and non-absorbing particles, the total scattering coefficient can be calculated theoretically (Morel, 1973) as the product of the geometrical cross-section of the particles per unit volume and a scattering efficiency factor. For the total scattering coefficient we thus have

$$T(z) = N(z)\pi \int_0^\infty Q(R) R^2 P(R;z) dR, \qquad (10)$$

in which the scattering efficiency factor is

$$Q(R) = 2 - 4 \frac{\sin(\sigma(R))}{\sigma(R)} + 4 \frac{1 - \cos(\sigma(R))}{\sigma^2(R)},$$

with

$$\sigma(R) = 4\pi R \frac{n - 1}{\lambda}.$$

According to Morel (1973) we used a mean index n=1.03, and a wavelength λ=0.643 μm which agrees with our apparatus.

4. RESULTS AND COMPARISON WITH OBSERVATIONS

In the previous section the settling velocity, the size-rate and the particle size-distribution just below the biologically active surface layer were specified. The volume density distribution and the total light-scattering coefficient were defined. On account of this we are now able to compare theoretical results with observations. In sections 4.1 and 4.2 we will restrict our attention to the stationary state of the particles above the clear water minimum, and in section 4.3 we will discuss the effect of the remobilisation of particles from the bottom.

4.1 The volume density distribution

The theoretical volume density distribution calculated from (9) is shown in fig.2 at five different depth-levels. Since the weight coefficient in (8) is small, the first mode strongly dominates in the subsurface layer (fig.2a,b). The small particles dissolve and slow down progressively. The larger particles descend faster and add more to the volume density. Consequently, the distribution flattens out as the depth increases (fig.2c). This flattening out

of the volume density distribution has been reported by several authors, among which Brun-Cottan (1971), Sheldon *et al.* (1972), McCave (1975, 1983), Lerman *et al.* (1977), and Pak *et al.* (1980). In the deep layers, the second mode starts to dominate the volume density distribution (fig.2d,e). This is in contrast with observations. This suggests that the influence of particles originating from the bottom is not negligible, as discussed in section 4.3.

4.2. The nephelometric profiles

Vertical profiles of the theoretical total light scattering coefficient calculated from (10) are shown in fig.3. The scattering was normalized at depth z=100 m, where the input particle size-distribution is defined. Since there is only an input of particles at this depth, no bottom influence is included. The effect of the dissolution-rate ε is illustrated by the change in shape of the profiles. When the dissolution-rate is high, particles dissolve relatively fast, and the corresponding profiles decrease rapidly with depth over the first few hundred meters. For a low dissolution-rate the profile's gradient weakens in the upper part of the ocean, and if the dissolution-rate tends to zero, the corresponding profile tends to a straight vertical line. In this extreme case, the particle distribution becomes independent of depth.

It is mentioned that the shape of the profiles is primarily determined by the first mode of the particle size-distribution (8), i.e., the mode that was fitted with the usual power law distribution. Because large particles descend relatively fast, they have no time to dissolve considerably in the subsurface layer. Therefore, the influence of the second mode is mainly to establish the 'curtain effect' mentioned in 3.1. Further, it is remarked that Munk's background velocity of the fluid (Munk, 1966), compared to no background velocity at all, has hardly any influence on the shape of the curves as well, since its magnitude

is small. A background velocity becomes important when remobilisation of particles from the turbulent bottom boundary layer is considered (see section 4.3), or when the resulting stationary state of the dissolved mass due to dissolution of particles is being looked at, since without a background velocity, the mass-density of the dissolved mass would tend to infinity everywhere in water-column. (The distribution of the dissolved mass in the water-column due to the dissolution of particles is readily derived by applying the conservation of mass law in section 2.2 and by integrating over all radii with the results obtained in section 2.3).

The characteristics of nephelometric profiles measured in the North-East Atlantic around $47^{\circ}N/20^{\circ}W$ were studied within the framework of the NOAMP experiment (Nordost- atlantisches Monitoring- Programm) and were described by Nyffeler and Godet (1986). In summer 1989, repeated nephelometric measurements were performed at a single location, within the framework of the JGOFS pilot study. The home-made nephelometer used in the experiments is based on the principle of light forward-scattering. For marine particles, the variations in the shape of the angular scattering function are small, and scattering around $4^{\circ}-5^{\circ}$ offers the best proportionnality with the total scattering coefficient defined in section 3.3 (Morel 1973). The apparatus was calibrated versus a standard Formazine solution, and the results in fig.4 are expressed as equivalent turbidity units (mFTU = milli Formazine Turbidity Unit). In fig.4 fifteen profiles obtained during the JGOFS experiment are overlapped. The comparison of the trend in the measured profiles with the theoretical profiles in fig.3 confirms that ε=0.15 μm/y (which is the dissolution-rate for calcite particles taken in section 3.1) is indeed a reasonable value.

4.3 The bottom influence

The discrepancy between the observations (fig.4) and the

calculated profiles (fig.3) becomes evident below the clear water minimum. We consider two factors that might be important. As suggested by Brewer *et al* (1976), isopycnal transport of particles may be a first cause. Horizontal isopycnals do in principle not influence theoretical results, since then the open ocean system remains horizontally homogeneous (see section 2.1). However, in case the isopycnals are not horizontal, particles may be transported from the surface to deeper layers in a relatively short time. The second factor, and as we believe the more important one in the NOAMP area, is the bottom influence. In case of an upward background velocity u, particles with radii smaller than $R=\varkappa$ (section 2.2) are remobilized from the turbulent bottom boundary layer (BBL), since their movement is upward. Although the mean vertical velocity over a long period of time may well be zero (or the one mentioned by Munk (1966)), temporary fluctuations of u may be considerable. Since a downward background velocity does imply zero remobilization, fluctuations of u around its mean value induce a net effect of particle remobilization from the BBL. Indeed, numerous benthic storms related to deep reaching synoptic eddies have been observed in the NOAMP area over a relatively small period of time (Klein, 1987), which implies that these storms are not exceptional. Thus, the lower part of this ocean-region is at times rather energetic and the vertical background velocity near the bottom can not be considered to be a stationary quantity. This is in conflict with the stationary state hypothesis. Over a long period of time we might however consider the background velocity to be a random variable, for example normally distributed with zero mean and with variance related to the vertical kinetic energy. Instead that the background velocity with respect to a particle be a function of time, we may assume that the problem is equally well described by saying that the background velocity for each particle is constant, but that different particles may have have different background velocities according to the background velocity's distribution. It is beyond the scope of this paper to justify this ergodic argument thouroughly. Simply, by specifying a particle repartition at the top of the BBL and one upward background velocity that allows the

particles to rise towards the observed clear water minimum level which is about 1500 m above the bottom (see fig.4), we obtain the turbidity profile shown in fig.5. The used value for the background velocity is fifty times Munk's value (Munk, 1966), i.e., u=7 μm/s. For this value, particles with radii smaller then R=$\varkappa$=3.10μm are remobilized from the BBL. They dissolve during their upward movement with a constant rate ε=0.15 μm/y. Munk's background velocity is retained for particles that come from the surface.

5. CONCLUDING REMARKS

Four major categories of processes have been looked at with respect to the changes in size of particles in the oceans: dissolution, adsorption, splitting and aggregation. By considering the size-rate and the vertical settling velocity to be functions of the particle's radius, the stationary state distribution of particulate matter as a function of depth was derived in case of the dissolution- process. In case of adsorption, splitting and aggregation, analogeous derivations can be made. The resulting expressions determine the state of the particle population in a horizontally homogeneous open ocean system, when the number of particles per unit volume and the particle size-distribution at the surface and/or at the bottom are prescribed.

By only considering dissolution of particles, we were able to restore, on a theoretical basis, the typical features of turbidity profiles and volume distributions that are observed in open ocean systems. Although all particles have the same constant dissolution-rate in the calculations (which is a rather strong simplification compared to reality), the results confirm the validity of the present approach. The presence of marked bottom nepheloid layers repeatedly observed in the NOAMP area can be related to the fact that the vertical kinetic energy is relatively high in that region. Remobilisation of small particles from the BBL and their subsequent dissolution would be sufficient to

explain the thickness of the nepheloid layer below the clear water minimum.

ACKNOWLEDGEMENTS

This research was performed within the framework of the PROSPER program (University of Neuchâtel, Switzerland) with the support of the Swiss Environmental Protection office and the Swiss National Science Foundation (grant nr: 2.055.0B6). We thank B.Kübler, O.Besson, R.Laydi, T.Adatte, G.Rumley, C.H.Godet, X.Durrieu de Madron and R.Jantschik of the University of Neuchâtel for their critical comments and stimulating enthusiasm.

REFERENCES

Bader H. (1970). The hyperbolic distribution of particle sizes. Journal of Geophysical Research, 75, 2822-2830

Batchelor G.K. (1967). An Introduction to Fluid Dynamics, Cambridge University Press.

Biscaye P.E. and S.L. Ettreim (1977). Suspended particulate loads and transports in the nepheloid layer of the abyssal Atlantic. Marine Geology, 23, 155-172.

Brewer P.G., D.W.Spencer, P.E.Biscaye, A.Hanley, P.L.Sachs, C.L.Smith, S.Kadar and J.Fredericks (1976). The Distribution of Particulate Matter in the Atlantic Ocean. Earth and Planetary Science Letters, 32, 393-402.

Brun-Cottan J.C. (1971). Etude de la granulométrie des particule marines, mesures effectuées avec un compteur Coulter. Cahier Océanographiques, 23, 193-205

Brun-Cottan J.C. (1976). Stokes settling and dissolution rate model for marine particles as a function of size distribution. Journal of Geophysical Research, B1, N°9, 1601-1606.

Ettreim S.L, E.M.Thorndike and L.Sullivan (1976). Turbidity in the Atlantic Ocean. Deep-Sea Research, 23, 1015-1027.

Klein H. (1987). Bentic Storms, and Particle Dispersion in the Deep West European Basin. Dt.hydrogr.Z.40.

Lal D. (1977). The Oceanic Microcosm of Particles. Science, Vol.198, Nr.4321, 997-1009.

Lambert C.E., C.Jehanno, N.Silverberg, J.C.Brun-Cottan and R.Chesselet (1981). Log-normal distribution of suspended particles in the open ocean. Journal of Marine Research, 39, 77-98.

Lerman A., D.Lal and M.F.Dacay (1974). Stokes' settling and chemical reactivity of suspended particles in natural waters. in: Suspended Solids in Water, edited by R.J.Gibbs, pp. 17-47, Plenum, New York.

Lerman A., K.L.Cardner and P.R.Betzer (1977). Elimination of fine suspensoids in the oceanic water column. Earth and Planetery Science Letters, 37, 61-70.

McCave I.N. (1975). Vertical flux of particles in the ocean. Deep-sea Research, 22, 491-502.

McCave I.N. (1983). Particulate size spectra, behaviour and origin of nepheloid layers over the Nova Scotian Continental Rise. Journal of Geophysical research, 88, 7647-7666.

McCave I.N. (1984). Size spectra and aggregation of suspended particles in the ocean. Deep-Sea Research, Vol 31, N°4, p329-352.

Morel A. (1973). Diffusion de la lumière par les eaux de mer. Résultat expérimentaux et approche théorique. in: Optics of the Sea/ Lectures serie 61/ 3.1.1-3.1.76, AGARD-NATO Brussels.

Nyffeler F. and C.H.Godet (1986). The structural parameters of the benthic nepheloid layer in the Northeast Atlantic. Deep-Sea Research, 33, 2, 195-207.

Nyffeler F. and P.Ruch (1989). Size distribution of the suspended particles in the water masses of the Northeast Atlantic. in: Interim oceanographic description of the North-East Atlantic dumpsite for radioactive waste / OCDE Paris, 1989.

Pak H., J.R.V.Zaneveld and J.Kitchen (1980). Intermediate nepheloid layers observed off Oregon and Washington. Journal of Geophysical Research, 85, 6697-6708.

Sheldon R.W., A.Prakash and W.H.Sutcliffe (1972). The size distribution of particles in the ocean. Limnology and oceanography, 17, 327-340.

FIGURE CAPTIONS

Fig.1. Schematic survey of the four categories of processes.

Fig.2. Evolution of the theoretical volume density distribution with depth as a consequence of dissolution (ε=0.15 μm/y) only (without influence of the bottom).

Fig.3. Normalized theoretical profiles of the total light-scattering coefficient, calculated for varies dissolution-rates (without influence of the bottom).

Fig.4. Composite plot of fifteen nephelometric profiles measured around 47°N/20°W during the period 10-08-'89/25-08-'89.

Fig.5. Normalized theoretical light-scattering profiles with a dissolution-rate of ε=0.15 μm/y, calculated with (solid line) and without (dashed line) bottom-influence.

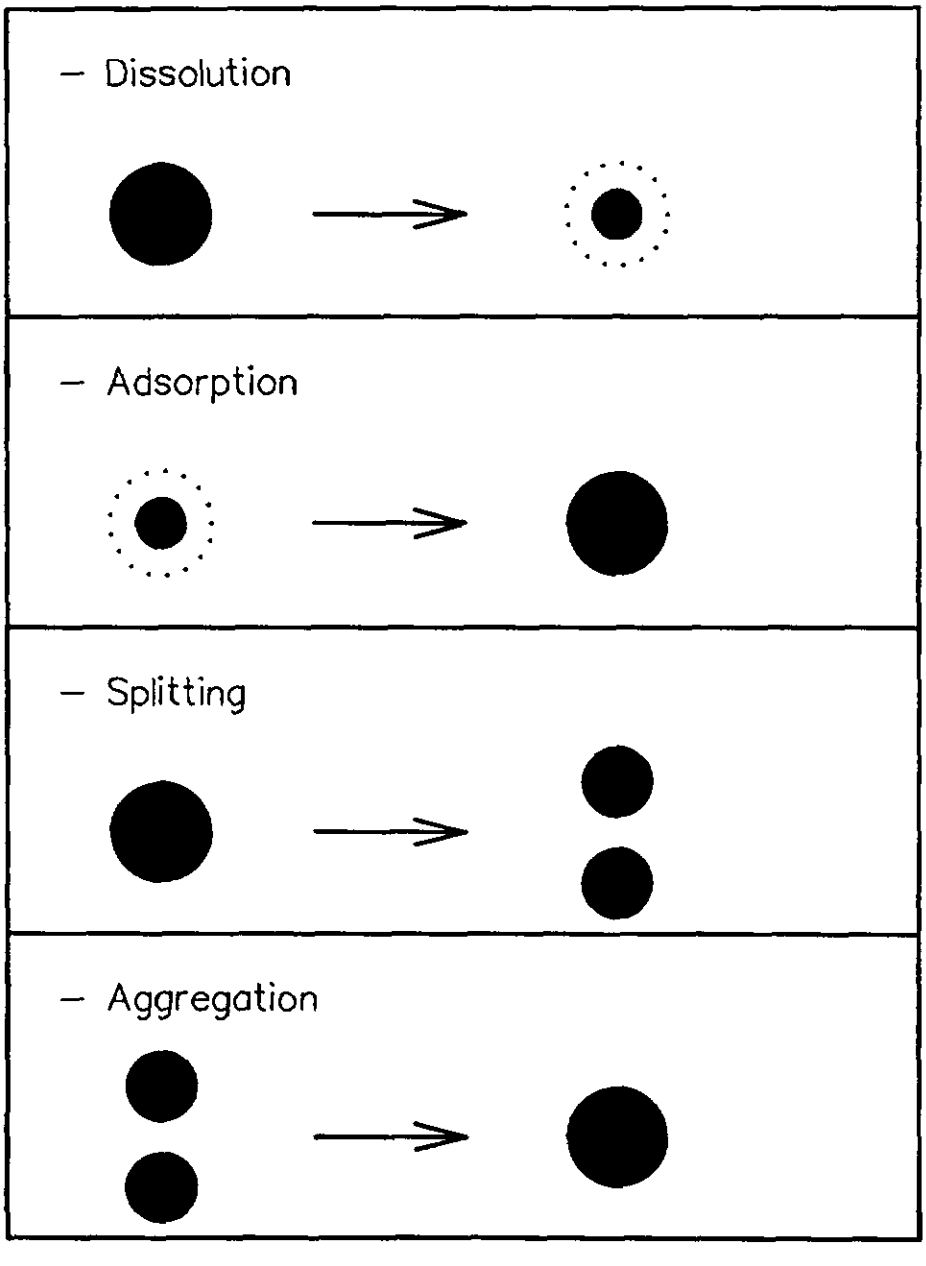

fig. 1

fig.2.

Volume distribution

Plotted radius interval
between 0.75 and 15.0 micron.

$P_v = [1/V(z)][\partial V(z;R)/\partial R]$

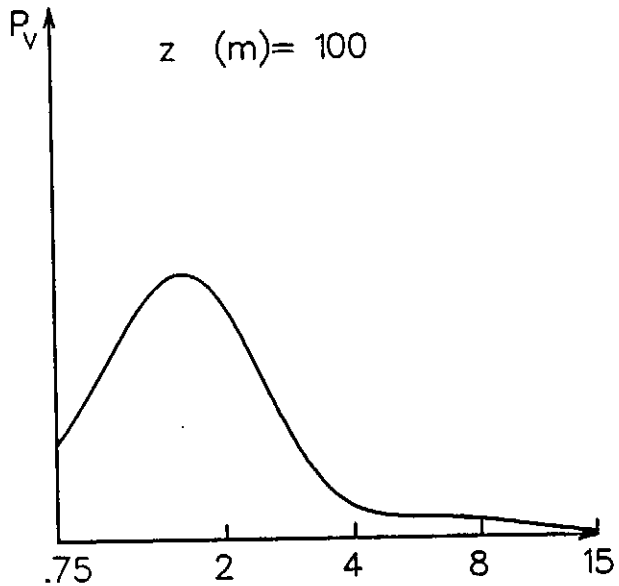

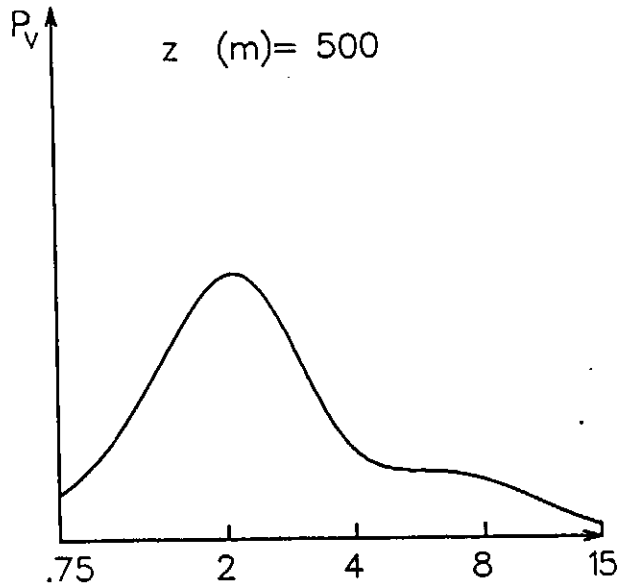

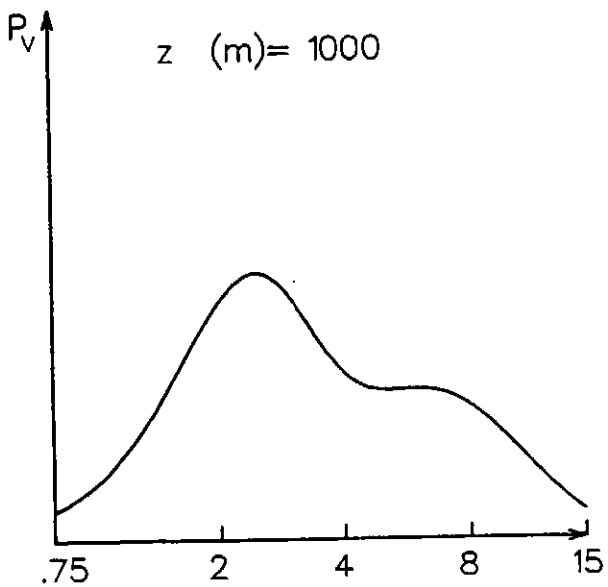

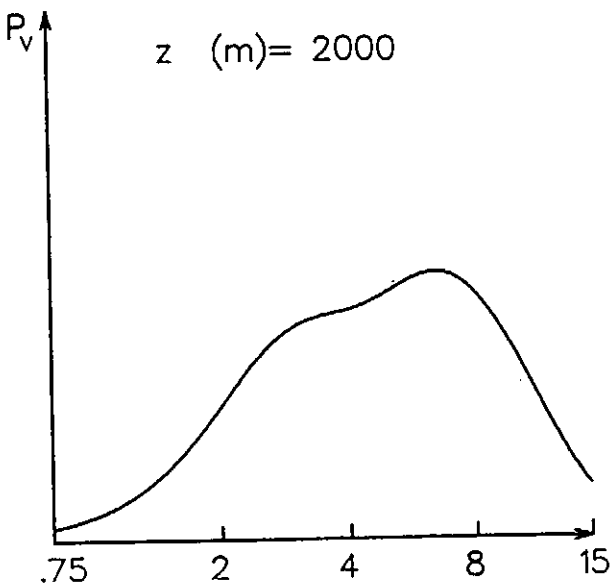

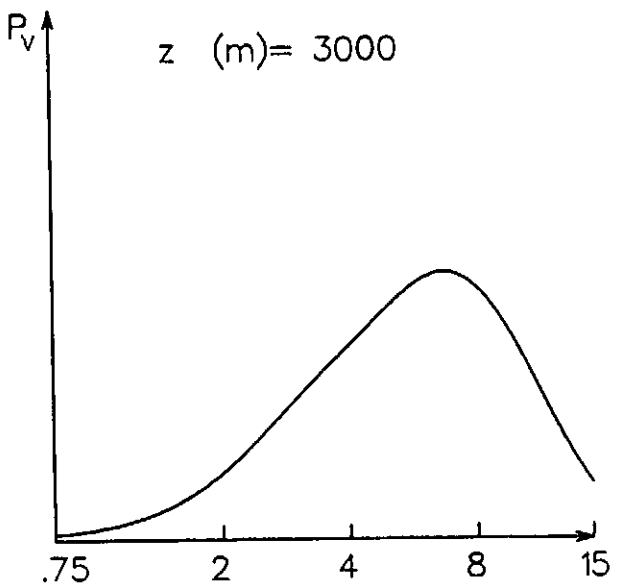

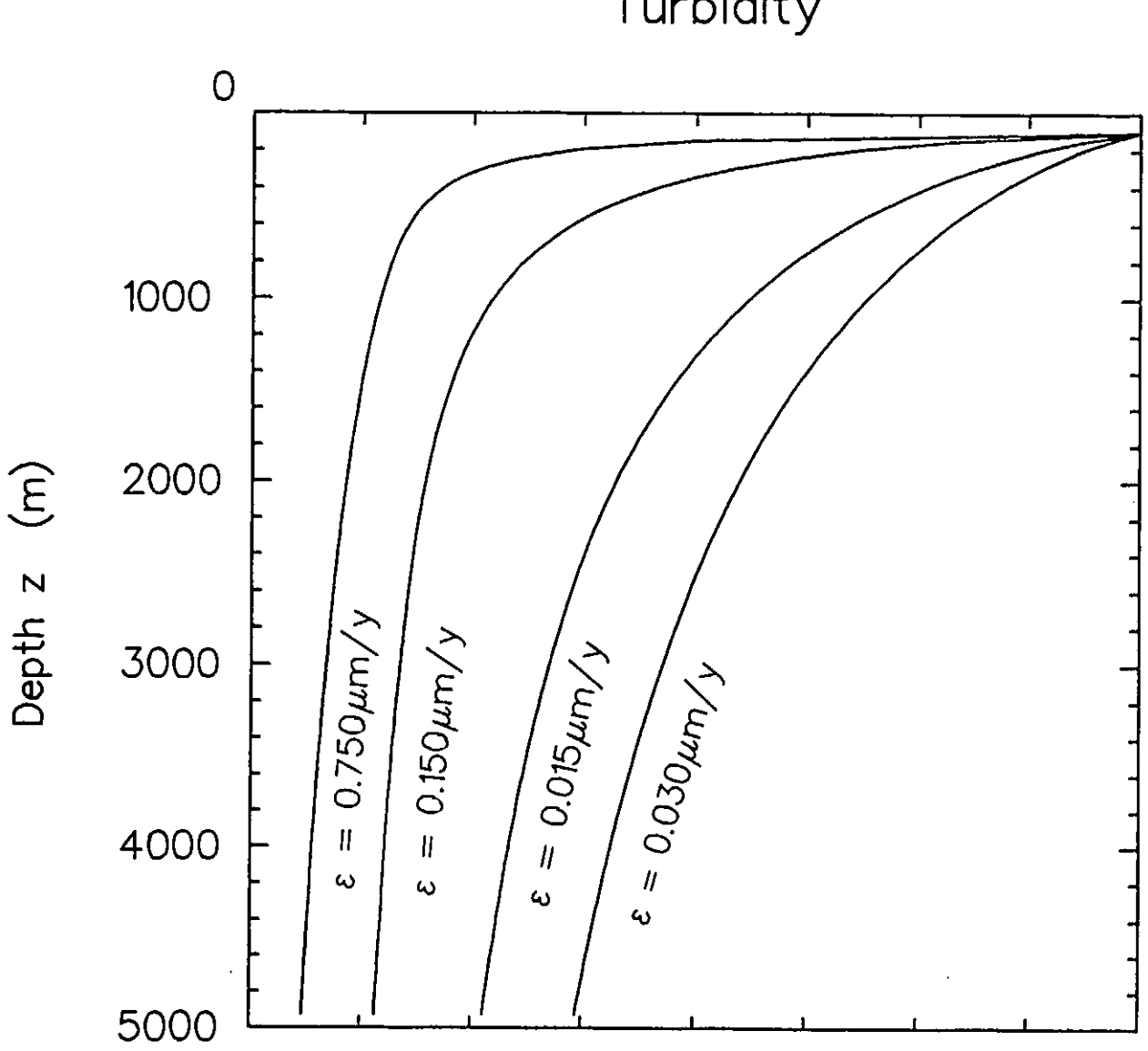
Turbidity
0
1000
2000
3000
4000
5000
Depth z (m)
ε = 0.750μm/y
ε = 0.150μm/y
ε = 0.015μm/y
ε = 0.030μm/y

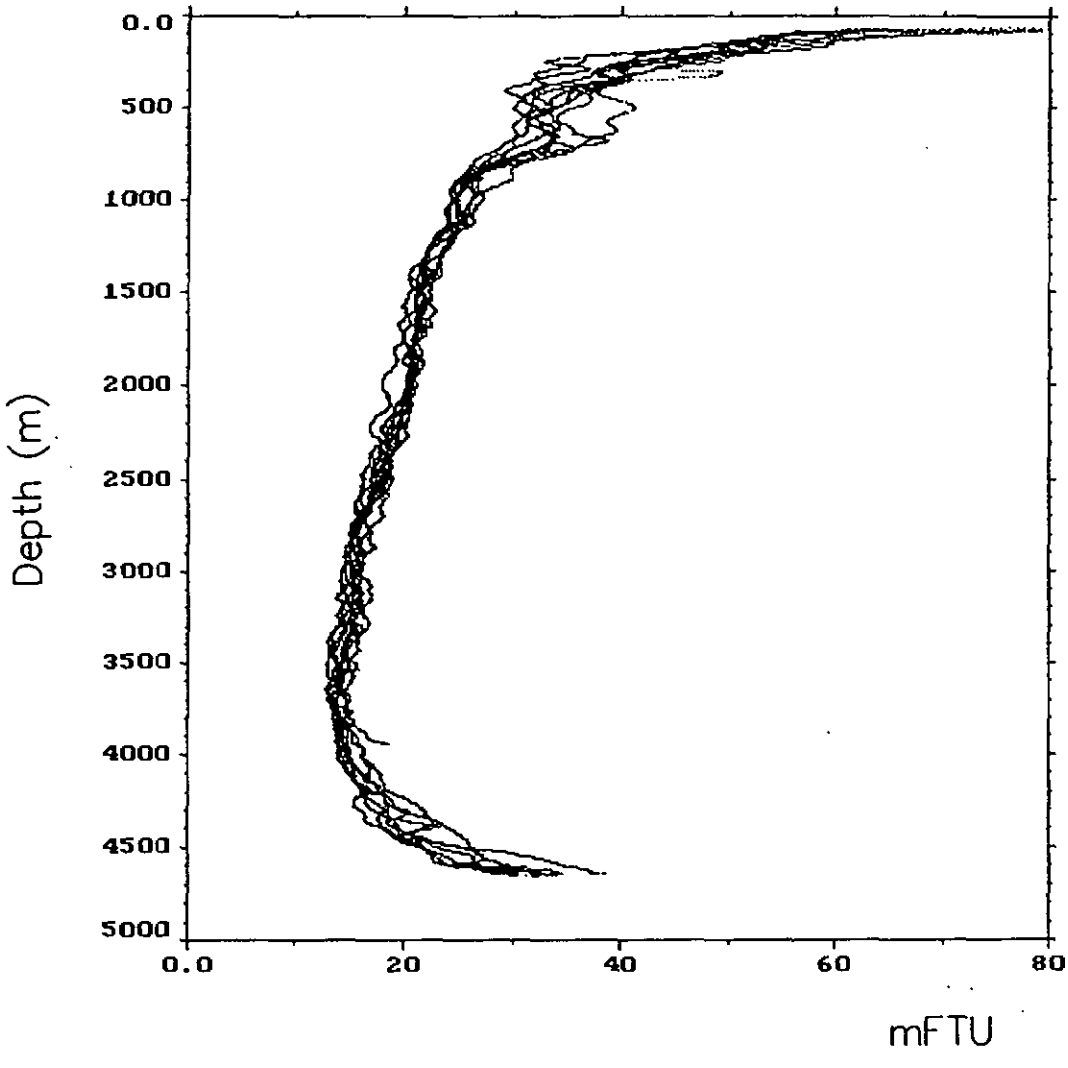
0.0
500
1000
1500
2000
2500
3000
3500
4000
4500
5000
Depth (m)
0.0
20
40
60
80
mFTU

fig. 4.

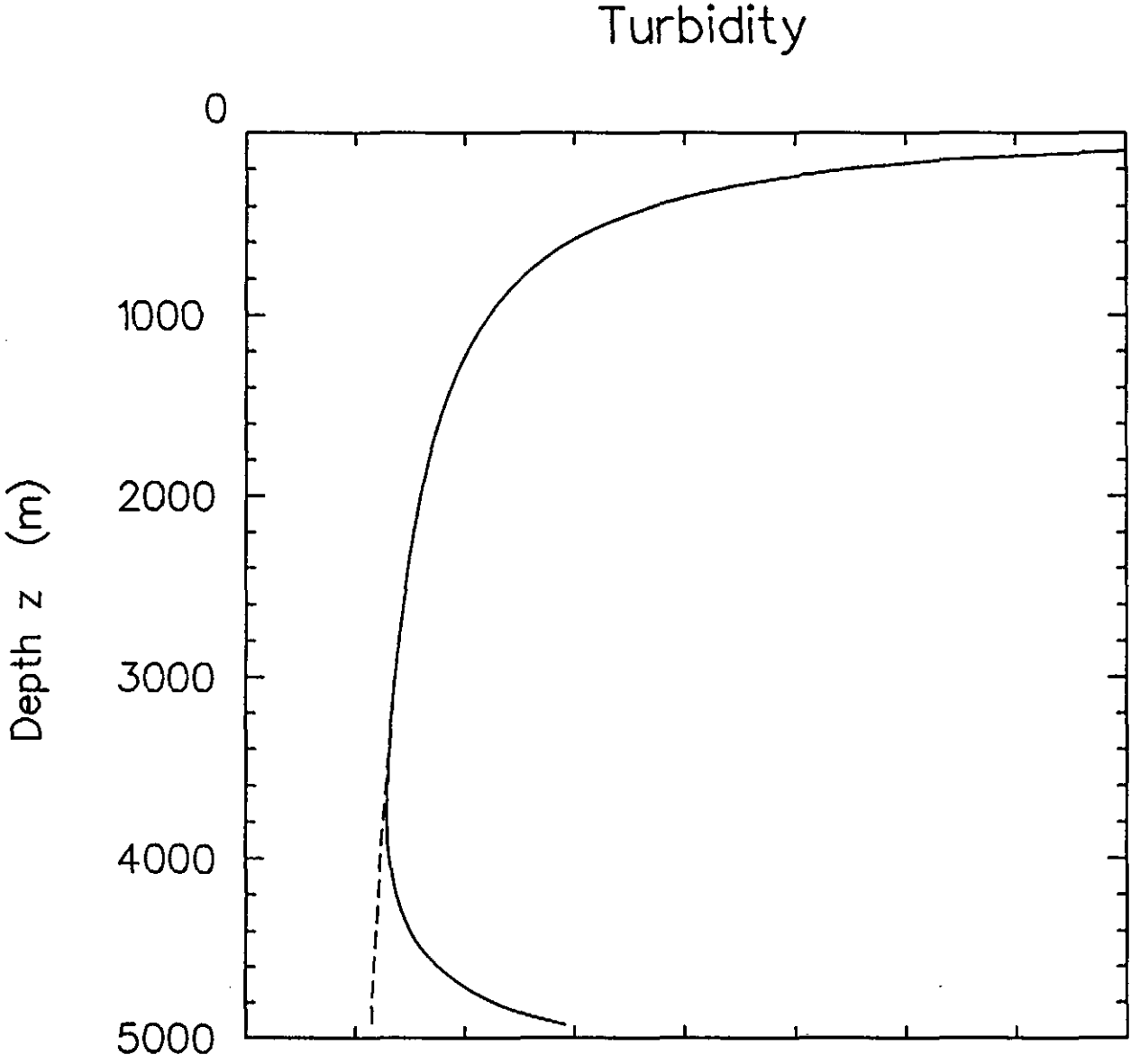

Fig. 5.